

RELATIVISTIC QUARK PHYSICS

Johann Rafelski

Department of Physics, University of Arizona, Tucson, AZ, 85721

We present a brief survey of the development of nuclear physics towards relativistic quark physics. This is followed by a thorough discussion of the quest for the observation of the dissolution of nuclear matter into the deconfined quark matter (QGP) in relativistic nuclear collisions. Use of strange particle signatures in search for QGP is emphasized.

1 From Nuclear to Quark Physics

What (we think) we know and what we know we do not know

The atomic nucleus is a quantum bound state of nucleons (protons and neutrons) each comprising three confined i.e. permanently bound valance quarks. The dynamics of nearly massless quarks $q = u, d$ inside a nucleon is fully relativistic. Thus the mass of the nucleon and hence of the nucleus, and therefore of about 98% of all matter known to us, is understood to be the relativistic quark quantum-zero-point energy. Confinement localizes quarks to within a volume with radius of about 1 fm in size, about 20–40 times less than (light $q = u, d$) quark Compton wavelength $\lambda(q) = \hbar c/m_q$, with $3 < m_q < 15$ MeV. Most important point here is that the indirectly arising interactions, due to the properties of the confining strongly interacting vacuum state, determine the scale of hadronic size, and thus mass, and thus all the properties of the Universe we see around us. Moreover, as we shall argue at the end, there is all reason to believe that the hadronic energy scale is a direct descendent the unification scale of gauge interactions.

Research of past 50 years, since the discovery of the pion¹, established the following paradigm of the properties of strong interactions^{2,3}: $SU(3)_c$ -QCD is the fundamental gauge theory of strong interactions, with quarks q and gluons G being the *color* charged fundamental degrees of freedom; all strongly interacting and in our vacuum mobile particles are color neutral. To explain the confinement of colored states to localized region of space time the principal postulate is⁴ that the *true* vacuum state $|V\rangle$ abhors the color charge; but there is an excited state $|P\rangle$ referred to as *perturbative vacuum* in which colored q, G particles are mobile and have their naive perturbative physical relevance.

The physical difference between $|P\rangle$ and $|V\rangle$ is akin to the difference between vapor and ice; in regions of space-time in which ‘elementary’ vapor exists, where $|P\rangle$ replaces $|V\rangle$, a finite energy density the latent heat \mathcal{B} has

Table 1: Strong interaction vacuum states

vacuum	state	E/V [GeV fm ⁻³]	m_q [MeV]
true	$ V\rangle$	0	∞
fluid flavor	$ F\rangle$	$\mathcal{B}_F = 0.1$	350
perturbative	$ P\rangle$	$\mathcal{B}_P = 1$	5–15

been deposited. Pushing the vapor and liquid phase similarity we see that there may be an intermediate state of the vacuum which we shall call $|F\rangle$. In this ‘fluid flavor state’ the color quantum numbers of quark and gluons are mobile, but the dissolution of $|V\rangle$ is not complete, and relatively little latent heat is consumed in the transformation $|V\rangle \rightarrow |F\rangle$. The principal degrees of freedom in the $|F\rangle$ -vacuum could be effective ‘constituent’ quarks.

Thus to dissolve fully the quantum vacuum structure a considerable latent (condensation) heat per unit volume needs to be delivered. It is thought that it is of the magnitude $\mathcal{B}=0.1\text{--}1$ GeV fm⁻³. The lower value $\mathcal{B}_F = 0.1$ GeV fm⁻³ is the energy scale required for the understanding of hadron masses (see Section 2), the upper value $\mathcal{B}_P = 1$ GeV fm⁻³ arises aside from lattice gauge studies of QCD⁵ from the necessity to make the deconfining, perturbative state $|P\rangle$ inaccessible in low energy reactions, in which free quarks and gluons do not become apparent as the fundamental degrees of freedom. \mathcal{B}_F is the dimensioned quantity which determines the hadronic mass and size scales. The value of $\mathcal{B}_F = 0.1$ GeV fm⁻³ has to be compared to ‘normal’ matter condensation energies which have a magnitude of say 0.1eV Å⁻³, a factor 10²⁴ smaller! In order to study states with extreme properties rivaling those found in early Universe some 40 μ s after its birth we have developed experimental facilities in which heaviest nuclei are made to collide at high energies.

Unclear horizons

There are many open questions and unresolved puzzles in relativistic quark physics. Some are fundamental and border on the comprehension of the origin of the standard model, other are simply consequences of the complexity of the gauge theory that governs quantum-chromodynamics (QCD), the theory of strong interactions.

- The fundamental questions are of the type: why do quarks have so many different quantum numbers, e.g. i) fractional electrical charge, ii) color non-Abelian charge, iii) several (three) families of particles, where (u, d) , (c, s) and (t, b) are the three doublets of quarks, iv) intrinsic spin. However, an elementary object is expected to possess just a few simple properties. Are perhaps even quarks not elementary?
- Understanding of quark confinement riddle falls under the practical category of solving QCD. It is not merely the problem of the vacuum properties, but significantly, a problem of hadronic spectrum. The key problem that emerges is that we cannot find experimentally many of the bound states of quarks that intuitive extrapolations of the current understanding imply.

Diverse simple quark bound states other than known mesons and baryons corresponding to angular and radial quark excitations inside the confining boundary are absent. Other expected states, such as the nucleon-anti-nucleon molecule (baryonium) which in the quark language consists of the spatially separate two quark – two antiquark clusters, $qq-\bar{q}\bar{q}$, have also not been seen.

The nucleus is made of $3N$ quarks, but quarks remain clustered in nucleons. Why are quarks not seen to bind other than in clusters of three? How much excited would be the state comprising $3N$ freely movable quarks? In a two-vacuum model this is a state that should be nearly stable. But it is hard to imagine formation of dense quark matter without allowing for heating during compression in collision of heavy nuclei. At finite temperature we have some quark-antiquark pairs and real gluons appear. This is the quark-gluon plasma (QGP) state of matter last seen in the early Universe. In the limit that color charge interactions of quarks and gluons are small, which we believe to be the case in non-Abelian gauge theories at high energies, given the decrease in strength with energy scale of the coupling constant, the relativistic quantum gas properties only depend on the number of excitable degrees of freedom, that is the degeneracy g and the kinematic relation between energy and particle momentum.

It is of course far from certain that the QGP can or/and will be created in relativistic nuclear collisions which last just an instant, as short as light needs to cross a nucleus, 10^{-22} s. Our hope and expectation is that in a statistical system with many degrees of freedom at as high a temperature as $kT = 150\text{--}250$ MeV, the detail of hadron dynamics and structure that escaped our attention will become irrelevant and we will be able to observe properties of deconfined nuclear matter. It is possible that the complex aspects of interactions within confined bound states become irrelevant in the high

density/energy limit. The question then is under what conditions we actually encounter this asymptotic limit, and what, if anything, we can learn when studying the approach to this limiting case.

We shall address here several issues that we left open in our report made at the last meeting⁶ and we shall attempt to make an elementary presentation accessible in a large part to students; however, we recommend that the second half of this paper be read in conjunction with our earlier report⁶, as it continues and updates the developments reported. Before proceeding with more rigorous discussion of the vacuum and hadronic structure in Section 2, we shall give next a brief historical reminiscence about relativistic nuclear physics. Recent aspects of quark-gluon plasma studies are introduced in Section 3. We describe the considerable progress that has occurred in past two years regarding strange particle flavor production in Section 4. The still preliminary discussion of particle production in hadronizing QGP is offered in Section 5, where we also compare with recent Pb–Pb 158 GeV A CERN heavy ion collision experimental results. We conclude this report with a discussion of the ongoing research work.

Historical remarks

The discovery of natural radioactivity more than 100 years ago occurred when both quantum mechanics and relativity, the two pillars of our current quest for quark physics, were not yet formulated in their final form. Relativity and nuclear physics evolved initially without mutual interaction. Quantum physics was applied rapidly to understand puzzles of nuclear physics, a good example is the α -decay using quantum tunneling. Relativity enters with Fermi theory of β -decay: ‘...in order to obtain relativistically invariant form ... necessary at the velocities of emitted electrons close to velocity of light... we must use Dirac four functions...’ writes George Gamov in *Structure of Atomic Nuclei and Nuclear Transformations* published 60 years ago. This is perhaps the first textbook mention of relativity within nuclear physics.

Hideki Yukawa proposed a theoretical yet undiscovered particle, the meson, as the origin of short range nuclear interactions. This bold step generated a lot of interest in fundamental understanding of nuclear forces and nuclei, which continues to this day. After the initial confusion caused by the unexpected heavy electron, the muon, the discovery of the π -meson in 1947¹ by Lattes, Occhialini and Powell just 50 years ago today made the odd couple, relativity and nuclear physics, inseparable. With this discovery a novel interpretation of the nucleon-nucleon interaction came immediately within range. Already in 1948, Rosenfeld’s book *Nuclear Forces* describes the Breit-type reduction of the fundamental meson interaction to the effective nonrelativistic form, involving

the spin-orbit coupling.

Since there are several mesons, generalization of Yukawa ideas involve nucleon-nucleon interactions with different Lorentz transformation symmetry, from which the nuclear shell model potential arises, given that the range of the interaction is the mean distance between nucleons in nuclei. In magnitude, the effective single particle nucleon potential V_{eff} in the nucleus is not much bigger than a few percent of nucleon mass m_N , as is born out by Bethe-Weizsäcker mass formula which gives the bulk nuclear binding energy at about 15 MeV/nucleon, less than 2% of m_N . However, the spin-orbit coupling influence on nucleon energies is in comparison surprisingly big, as is born out by study of nuclear spectra. Relativity provides here a rather simple explanation of a fundamental puzzle of nuclear physics, and also explains how it can happen that strongly interacting nucleons are bound by a relatively small potential. At this point relativity becomes inseparable part of nuclear physics.

The solution of this puzzle requires consistent Breit reduction of relativistic wave mechanics to non-relativistic limit, schematically:

$$V_{\text{eff}} \simeq \{-U + V\} + \frac{1}{2m_N^2 r} \frac{d}{dr} \{U + V\} \vec{L} \cdot \vec{S} + \dots \quad (1)$$

We see that the spin-orbit force is the sum of the gradients of the (pseudo)scalar U and vector meson V exchange potentials, while the radial part of the effective potential for the nucleons is the difference of both these contributions $V - U$. This than explains the relatively small nuclear shell potential, now understood as the difference $V - U$, as U, V can be large as long as their magnitude is similar. Indeed, we can have complete absence of spin-orbit coupling ⁷ when the V, U potentials add and thus the $\vec{L} \cdot \vec{S}$ -coupling term vanishes, while the opposite limit in which the (nearly) exact cancelation of the V, U potentials, and the associated maximum of the $\vec{L} \cdot \vec{S}$ occurs, is the interesting property of nuclear interactions. Today, we believe that these nuclear interactions are the ‘unscreened’, van der Waals-type forces between quarks confined to individual nucleons. Efforts continue to obtain QCD-quark physics based derivation of the residual nuclear interactions.

The development of nuclear matter theory, neutron matter in neutron stars ensued in parallel with studies of high energy cosmic ray reactions. These two initially separate developments were precursors to our present day interests in hot nuclear matter, and ultimately hot hadronic matter, that is nuclear matter at so high temperature that it contains a significant meson abundance. On the other side, there was early recognition among particle physicists that elementary collisions involving strongly interacting particles lead to multi-particle production which could be described as if originating from a fireball of dense,

hot matter. Such theoretical work on multi-particle production by E. Fermi⁸ in USA, and L. Landau⁹ in Russia, which paved the way to the development in early sixties of statistical bootstrap model description of hadron production. Rolf Hagedorn, working out of CERN, has been since 1964 implementing a theoretical picture of particle production from boiling hot hadronic matter¹⁰. He was able to describe many experimental features of hadronic spectra within the newly developed statistical bootstrap model of dense hadronic matter comprising a resonance gas of point-like particles. Not only the properties of hadronic matter but also the hadronic mass spectrum emerged correctly from this approach. Ultimately, a connection has been established between particle and nuclear hot hadronic matter descriptions, by way of introducing into Hagedorn's bootstrap aside of 'elementary' mesons, also 'elementary' baryons of finite size¹¹.

In parallel to the development of phenomenological hadronic matter theory the fundamental understanding of hadronic structure was emerging. Just more than 25 years ago the present day stage was set when quantum-chromodynamics (QCD) was recognized as the fundamental gauge theory of strong interactions² from a number of other attempts to explain hadronic structure in terms of quarks. The development of hadronic structure within the MIT-bag model followed without delay¹², with constituents of nucleons, *up* and *down* quarks having in this approach just very tiny masses. To explain why the nucleon is so much more heavy than an electron an old model of the neutron has been resurrected: before the neutron discovery, the atomic nucleus was constructed from protons and tightly bound additional electrons. Without quarks this model could not work well since electrons were shown not to have strong interactions. Replacing the electrons with quarks which have indeed both strong and electric charge allows to describe the large masses of protons and neutrons in terms of the light elementary object, the 'electron' of QCD, the quark.

With light quarks as building blocks of hadrons, it took no time at all for Carruthers to propose the existence of "Quarkium: a bizzare Fermi liquid"¹³. Hagedorn extended his statistical bootstrap by considering the interior of hadrons, which were now understood as having a finite volume filled with light quarks. Under Hagedorn's guidance, I begun in 1977 at CERN to explore the melting/dissolution/fusion of dense and hot hadronic bootstrap matter into quark matter. One of the key issues is, if at the conditions of density and temperature, when confined, nucleon/meson type matter, reach the crossover point to the color conductive conditions of the vacuum we actually will encounter a phase transition. We soon arrived at a detailed description of the first order phase transition that we believed occurs between the confined and

deconfined phase¹⁴. Though this subject has since many times been revisited, this extension of the statistical bootstrap model to finite size hadrons with quark internal structure is still today the foundation of all detailed models of the dense hadronic matter formed in relativistic nuclear collision.

First conclusions: relativistic nuclear collisions

Looking back to these pioneering times of quark matter days the text of the abstract of the inaugural lecture of June 1980, which I presented at Frankfurt University comes to mind. It is quite short: *Quark Matter – Nuclear Matter*: ‘The fusion of the constituents – quarks — of protons and neutrons into quark matter, a new phase of nuclear matter, is expected to occur under experimentally accessible conditions of pressure and temperature.’

Our objective is to

- break up matter, freeing quarks, in laboratory experiments;
- study the Universe about $40\mu\text{s}$ after the Big-Bang by measuring properties of this hot, deconfined state;
- create a firm foundation of understanding of strong interactions in terms of a fundamental theoretical paradigm, confirmed experimentally.

Nearly certainly, there is some not yet understood principle at work that is needed to eliminate unobserved hadronic states. This is at the same time a challenge and an undesirable complication within this research program.

2 Quark Bag Model

Vacuum Structure

Among the most far-reaching developments of the recent 25 years of research into the consequences of fundamental interactions is recognition that the true physical vacuum is a state of considerable complex and physically significant structure. While we know that strictly speaking the vacuum is empty, its quantum structure (wave function) can be highly non-trivial, deviating considerably from that of a non-interacting Fock space. This is not the place to present the multitude of phenomena that go along with this effect, but we can illustrate some simple properties in order to justify the principal of confinement and the related appearance of light relativistic quarks in the description of the deconfined QGP. Indeed, one finds a quite remarkable comment to this point in Weinberg treatise³ (Volume II, p190, bottom) on Quantum Theory of Fields: ‘. . . this work was done without a specific theory of the strong interactions. One of the reasons for the rapid acceptance of quantum chromodynamics in 1973 as the correct theory of strong interactions was that it explained the $SU(2)\times SU(2)$

symmetry [inherent in Adler-Weisberger sum rule of 1965] as a simple consequence of the smallness of the u and d quark masses.’ So if quarks have a small mass, what is the origin of the 1 GeV scale of the mass of nucleons?

The infrared QCD instability leads to the appearance of a finite glue ‘condensate’ field i.e vacuum expectation value (VEV) of the gluon field-correlator^{15,16}, which is evaluated from experimental data to be:

$$\langle \frac{\alpha_s}{\pi} G^2 \rangle \simeq (2.3 \pm 0.3) 10^{-2} \text{GeV}^4 = [390 \pm 12 \text{ MeV}]^4, \quad (2)$$

here $\alpha_s = g^2/4\pi$ is the strong interaction (running) coupling constant, see Section 4, and

$$\frac{1}{2} G^2 \equiv \frac{1}{2} \sum_a G_{\mu\nu}^a G_a^{\mu\nu} = \sum_a [\vec{B}_a^2 - \vec{E}_a^2], \quad (3)$$

with $a = 1, \dots, N^2 - 1$ gauge field components in $\text{SU}_c(N)$. The value (and space-time shape) of the glue condensate has also been extracted from lattice gauge calculations¹⁷. It agrees well with the numerical value shown in Eq. (2), obtained from QCD sum-rules^{15,18}. Note that Lorentz and gauge symmetry of the vacuum state dictates that the VEV of a product of two field operators of the type shown here satisfy:

$$\langle G_{\mu\nu}^a(x) G_{\rho\sigma}^b(x) \rangle = (g_{\mu\rho} g_{\nu\sigma} - g_{\mu\sigma} g_{\nu\rho}) \delta^{ab} \frac{1}{96} \langle G^2(x) \rangle, \quad (4)$$

Taking the required contractions and using Eq. (3) one finds:

$$\langle \sum_a \vec{B}_a^2 \rangle = - \langle \sum_a \vec{E}_a^2 \rangle \quad (5)$$

Eq. (2) implies that $\langle \vec{B}_a^2(x) \rangle$ is positive, and $\langle \vec{E}_a^2(x) \rangle$ is negative. However, these signs are defined with reference to the perturbative state $|P\rangle$. Specifically, we are considering products of field operators which are normal-ordered with respect to $|P\rangle$ – where the condensate fields thus vanish by definition. The interpretation of Eq. (5) is that the B-field fluctuates in the true QCD vacuum $|V\rangle$ with a bigger amplitude than in the perturbative ‘vacuum’ $|P\rangle$, while the E-field fluctuates with a smaller amplitude than in $|P\rangle$: $|V\rangle$, the true vacuum, may be completely ‘magnetic’, without any electric fluctuations, while $|P\rangle$ may be completely ‘electric’, without any magnetic fluctuations. There are obviously many different ways to model and understand the glue condensate, and we shall not discuss this here in any greater detail. Within such models a

clear connection between the condensation energy \mathcal{B} and the glue condensate $\langle \frac{\alpha_s}{\pi} G^2 \rangle$ usually arises.

Another important property of the true vacuum has been shown well before the fundamental degrees of freedom and QCD have been understood. Expressed in modern language, the GOR-current algebra relation reads (see e.g.¹⁹):

$$m_\pi^2 f_\pi^2 \simeq -\frac{1}{2}(m_u + m_d)\langle \bar{u}u + \bar{d}d \rangle, \quad (6)$$

where u, d are the spinor field operators representing the two light quark flavor fields. The pion decay constant is $f_\pi = 93.3 \text{ MeV}$, and m_π refers to the charged pion mass $m_{\pi^+} = 139.6 \text{ MeV}$. The non-vanishing light quark masses $m_u + m_d$ are recognized to be the source of a finite mass of the pion; for vanishing quark masses the hadronic chiral $SU(2)_L \times SU(2)_R$ symmetry is realized in QCD is exactly. Current best estimate of the running QCD-current quark masses at 1 GeV scale are^{18,20,21}:

$$(m_u + m_d)|_{1 \text{ GeV}} \simeq 14.7 \pm 0.8 \text{ MeV}, \quad m_s|_{1 \text{ GeV}} \simeq 195 \pm 12 \text{ MeV}. \quad (7)$$

This light quark mass estimate arises from the GOR relation Eq. (6) and the quark condensate deduced from the properties of the vacuum:

$$\frac{1}{2}\langle \bar{u}u + \bar{d}d \rangle|_{1 \text{ GeV}} \equiv \frac{1}{2}\langle \bar{q}q \rangle|_{1 \text{ GeV}} = -[(225 \pm 9) \text{ MeV}]^3. \quad (8)$$

Model calculations^{22,23,24} employing mean field configurations of gauge fields in the QCD vacuum invariably suggest that it is the presence of the glue field condensate which is the driving force behind the appearance of the quark condensate. For example a specific model²⁵, (which employed a self-dual covariantly constant field) for the non-perturbative gauge field configurations in the structured QCD vacuum, finds that the quark condensation is a minor and stabilizing contributor (6%) to the vacuum energy due in its bulk part to the glue degrees of freedom. We further note that at high temperature the vacuum structure of QCD, as expressed by Eq. (2) in terms of the glue condensate, melts and one reaches the perturbative vacuum⁵. This confinement to deconfinement transformation and the chiral symmetry restoration as expressed by the melting of the quark condensate are seen at the same temperature.

It is thus generally assumed that the glue condensate is driving the quark condensate, and thus the large chiral symmetry breaking, despite the smallness of the quark masses. This is tantamount to the picture of quarks confined by glue fluctuations and the resulting large relativistic quark confinement energy. We now illustrate how presence of (fluctuating) gauge fields can induce

appearance of Fermion condensates. Schwinger in his seminal paper on gauge invariance and vacuum fluctuations [see²⁶, Eq. (5.2)] shows:

$$\langle \bar{\psi}(x)\psi(x) \rangle \rightarrow \frac{1}{2}\langle [\bar{\psi}(x), \psi(x)] \rangle = -\frac{\partial \Gamma[A_\mu]}{\partial m} \quad (9)$$

The left-hand-side of Eq. (9) defines here more precisely the meaning of the quark condensate in terms of the Fermi field operators at equal space-time point. The right-hand-side refers to the effective action density $\Gamma[A_\mu]$ of Fermions in presence of gauge potentials A_μ .

The one loop the effective action $\Gamma^{(1)}$ for constant gauge fields in the Abelian (QED) theory was already presented by Euler, Heisenberg, Kockel²⁷. We re-express this result using the invariant Maxwell-field-like-quantities E, B , which are related to the Maxwellian electric \vec{E} and magnetic \vec{B} fields by:

$$\begin{aligned} B^2 &= \frac{e^2}{2}\sqrt{(\vec{E}^2 - \vec{B}^2)^2 + 4(\vec{E} \cdot \vec{B})^2} - \frac{e^2}{2}(\vec{E}^2 - \vec{B}^2) \\ &\rightarrow |e\vec{B}|^2, \quad \text{for } |\vec{E}| \rightarrow 0; \end{aligned} \quad (10)$$

$$\begin{aligned} E^2 &= \frac{e^2}{2}\sqrt{(\vec{E}^2 - \vec{B}^2)^2 + 4(\vec{E} \cdot \vec{B})^2} + \frac{e^2}{2}(\vec{E}^2 - \vec{B}^2) \\ &\rightarrow |e\vec{E}|^2, \quad \text{for } |\vec{B}| \rightarrow 0. \end{aligned} \quad (11)$$

We also recall for later convenience:

$$\vec{E}^2 - \vec{B}^2 = -\frac{1}{2}F_{\mu\nu}F^{\mu\nu} \equiv -\frac{1}{2}F^2, \quad \vec{E} \cdot \vec{B} = -\frac{1}{4}F_{\mu\nu}\tilde{F}^{\mu\nu} \equiv -\frac{1}{4}F\tilde{F}, \quad (12)$$

where:

$$F^{\mu\nu} = \partial^\mu A^\nu - \partial^\nu A^\mu, \quad \tilde{F}^{\mu\nu} = \frac{1}{2}\epsilon^{\mu\nu\alpha\beta}F_{\alpha\beta} \quad (13)$$

In this notation the effective QED action to first order in the fine-structure constant $\alpha_e = e^2/4\pi$, and evaluated in the limit that the Maxwell field is constant on the scale of electron's Compton wave length (which is the situation for all externally applied macroscopic fields) is given by:

$$\Gamma^{(1)} = -\frac{1}{8\pi^2} \int_0^\infty \frac{ds}{s^3} e^{-m^2 s} \left[\frac{sE}{\tan sE} \frac{sB}{\tanh sB} - 1 + \frac{1}{3}(E^2 - B^2)s^2 \right]. \quad (14)$$

We note the two-fold subtraction required here: the first eliminates the field independent, zero-point action of the perturbative vacuum, and corresponds to normal-ordering of the field operators. The second subtraction is absorbed

in charge renormalization which assures that for weak fields the perturbative asymptotic series begins $\mathcal{O}(E^4, B^4, E^2 B^2)$. Schwinger²⁶ pointed out that the singularities along the real s -axis of the proper-time integral in Eq. (14) are related to instability of the vacuum due to pair production, a process in principle possible when potentials are present²⁸ that can rise more than $2m$, which is of course the case in presence of a constant, infinite range, electrical fields.

Employing Eq. (9) we obtain the condensate:

$$-m\frac{1}{2}\langle[\bar{\psi}(x), \psi(x)]\rangle^{(1)} = \frac{m^2}{4\pi^2} \int_0^\infty \frac{ds}{s^2} e^{-m^2 s} \left[\frac{sE}{\tan sE} \frac{sB}{\tanh sB} - 1 \right]. \quad (15)$$

We omitted here the renormalization of charge subtraction term [second subtraction in Eq. (15)] needed only for charge renormalization. Schwinger²⁶ reintroduced this specific term to obtain the leading effective electromagnetic interaction coupling of a neutral scalar meson to two photons.

There are few if any observable macroscopic effects of the fermion vacuum fluctuation in QED as these need to be induced by an extremely strong external force. In QCD situation is fundamentally different, due to spontaneous field fluctuations in the glue sector. To obtain a measure of the effects we need to substitute in the effective action Eq. (14) the pure U(1) Maxwell gauge field by the invariant combination of U(1) and the condensed SU(3) gauge fields:

$$\frac{\alpha}{\pi} F^2 \rightarrow \langle \frac{\alpha_s}{\pi} G^2 \rangle + \frac{\alpha_e}{\pi} q^2 F^2. \quad (16)$$

Here $q = 2/3, -1/3$ are the quark fractional Maxwell charges. In general one can ‘forget’ about the QED charges and proceed with QCD fields G alone. It is not appropriate to expand the effective action perturbatively since the QCD fields, even in the vacuum condensate, are in general more significant than the masses of light and strange quarks. When studying Eq. (15) one is rapidly lead to the conclusion that the mass of *light* quarks is not the important scale in the problem at hand, since for u, d, s quarks the glue condensate scale is greater than the quark mass.

We note that the substitution we have made in Eq. (16) implies when effected in the highly nonlinear function Eq. (15) that we have replaced

$$\langle G^{2n} \rangle \rightarrow (\langle G^2 \rangle)^n \quad (17)$$

which is correct under the tacit assumption that the fluctuations of the glue condensate can be understood as if generated by a background stochastic field^{17,29,30}. This is than the picture of the true QCD vacuum that we consider to be very promising model of the complex reality and which is implied in the following. The stochastic field fluctuations confine the color charges of quarks and gluons, and determine the confinement size.

Hadronic (Hyperfine) Structure

Without going much into well studied detail, the simple yet successful picture of hadronic structure is the ‘bag’-model. We view a hadron as comprising a spherical confining volume of radius R containing N -quarks in a bound state of mass M_N . Neglecting here the quark mass compared to the zero-point $1/R$ energy the bound state mass is given by:

$$M_N = \frac{\kappa N}{R} + \frac{4}{3}\pi R^3 \mathcal{B} + H_I. \quad (18)$$

The residual QCD interaction term H_I comprises the quark-quark interactions. The energy eigenvalue κ/R of the relativistic quark wave function with a boundary condition enforcing a vanishing current through the surface gives $\kappa = \kappa_c = 2.04$. The second term in Eq. (18) is the bag volume energy \mathcal{B} , the latent (condensation) heat of the vacuum. The balance of forces requires that the stationary state is at the minimum of $M_N(R)$ with respect to R , whence we determine the mass of the N -quark bound state:

$$M_N = (\kappa N)^{3/4} 1.755 \mathcal{B}^{1/4} \quad \text{for } H_I = 0. \quad (19)$$

If we fit the nucleon mass $M_3 = 940$ MeV by Eq. (19), than we find $\mathcal{B} \rightarrow \mathcal{B}_N^{1/4} = 140$ MeV, but working out the Δ -mass, $M_3 = 1330$ MeV one finds $\mathcal{B}_\Delta^{1/4} = 190$ MeV. These two values differ by factor 3.4 and thus we have to refine the approach. What is missing is the strong quark-quark interaction that is capable to generate the hadronic multiplet mass splitting. The color-electric quark-quark interaction is comparatively weak as the overall color charge of all hadronic states is zero, and only particles comprising both light and heavy quarks have a sizable static electric color charge density distribution. The color-magnetic hyperfine ‘spin-spin’ interaction term is¹²:

$$H_I = \sum_{i>j \in h} \langle h | \mu(r_{ij}) \frac{\lambda^i}{2} \cdot \frac{\lambda^j}{2} S^i \cdot S^j | h \rangle \quad (20)$$

Here $S = \sigma_a/2$, $a = 1, 2, 3$ is the spin vector of the two interacting quarks i, j , written in terms of the Pauli spin matrices σ_a , and $\lambda_a/2$, $a = 1 \dots 8$ is the generator of the color non-Abelian SU(3) charge. The dot product indicates summation over $a = 1, 2, 3$ for SU(2) and $a = 1 \dots 8$ for SU(3).

It turns out that all strongly interacting particles known (mesons and baryons such as π , ρ , N , Δ , K , Λ) can be consistently fitted using this color-magnetic interaction Eq. (20), see³¹. Let us recall here a ab-initio fit to all strange and non-strange mesons and baryons, allowing for massive strange

quark variable scale³² which produces $\mathcal{B}_b^{1/4} = 170$ MeV. In this fit also the quark eigenenergy κ was fitted, and the fitted value $\kappa = 1.97$ is nearly the theoretical value $\kappa_{\text{th}} = 2.04$, the small difference between theory and fit expected to arise from the distortion of the wave-function due to the hyperfine color-magnetic interaction. The spectra of hadrons tell us that quarks live in a relativistic, confined orbital, which fact supports the QCD-quark-confinement-vacuum structure picture of the nucleon.

Another success of both the relativistic and the non-relativistic quark bag model of hadrons is that we find that the most stable bound quark states have quantum numbers seen in stable hadrons, and that the mass hierarchy of flavor mass multiplets is correctly explained. This provides firm evidence that the interaction between quarks is obeying the rules of non-Abelian color-SU(3) algebra. To see this let us consider in more detail the situation for three quark states, i.e. baryons. We compute the strength of the chromo-magnetic interaction μ_I^h in Eq. (20), which we define as follows:

$$H_I = \delta E \mu_I^h; \quad \mu_I^h \equiv - \sum_{i>j \in h_q} \langle h_q | \frac{\lambda^i}{2} \cdot \frac{\lambda^j}{2} s^i \cdot s^j | h_q \rangle. \quad (21)$$

Signs are chosen such that $\delta E \propto 1/R$ is a positive quantity. μ_I^h can be positive or negative, depending on the quantum numbers of the bound state.

To obtain the value of the matrix element μ_I^h in a given hadronic state we follow here the permutation operator method³³. The exchange operator P_{ij} of two quarks is composed of three factors for spin, color and flavor quantum numbers, assuming that in the ground state the spatial wave function is identical for all quarks. For the totally antisymmetric quark state $|h_q\rangle$, for each quark pair i, j we have thus

$$P_{ij}^c P_{ij}^s |h\rangle = -P_{ij}^f |h\rangle; \quad P_{ij}^c = \frac{1}{3} + 2 \frac{\lambda^i}{2} \cdot \frac{\lambda^j}{2}; \quad P_{ij}^s = \frac{1}{2} + 2S^i \cdot S^j \quad (22)$$

The above explicit form of the permutation operators for the SU(2)-spin and SU(3)-color groups follows from the commutation properties of the generators $S = \sigma/2, \lambda/2$. Inserting Eq. (22) into Eq. (21) we obtain for the hyperfine interaction operator:

$$\mu_I = \sum_{i>j} \left\{ \frac{1}{4} P_{ij}^f + \frac{1}{24} + \frac{1}{4} \frac{\lambda^i}{2} \cdot \frac{\lambda^j}{2} + \frac{S^i \cdot S^j}{6} \right\}, \quad (23)$$

and naturally $\mu_I^h = \langle \mu_I \rangle$.

To complete the evaluation of μ_I we need to commit ourselves to the symmetry group governing the flavor exchange operator. Since strangeness is

well distinguishable from u, d flavors one can take the point of view that we should use only the light quark SU(2) flavor group with:

$$P_{ij}^{f_2} = \frac{1}{2} + 2I^i \cdot I^j, \quad (24)$$

and hence³³:

$$\mu_I = \frac{n(n-1)}{12} + \sum_{i>j} \left\{ \frac{1}{2} I^i \cdot I^j + \frac{1}{6} S^i \cdot S^j + \frac{1}{4} \frac{\lambda^i}{2} \cdot \frac{\lambda^j}{2} \right\}, \quad (25)$$

where we have used $\sum_{i>j} = n(n-1)/2$. We then have to account for the interaction of strange quarks with the non-strange quarks separately. It turns out that the fitted³² chromo-magnetic interaction energy δE_{qs} between strange and light quarks is half as large compared to u, d interactions, and that strange-strange chromo-magnetic interaction δE_{ss} is yet five times weaker than the u, d case. Such decrease of magnetic interaction is consistent with the expectations that the more massive quark has a smaller magnetic moment. While these results support the need to separately treat the light and strange flavors, we note in passing that if we had taken u, d, s quarks at par, than the larger SU(3)-flavor group would relate to flavor symmetry. Accordingly in that case one should evaluate³⁴ in Eq. (23) the flavor exchange operator using the quadratic Casimir of the SU(3)-flavor group to represent the flavor permutation operator in Eq. (22). We will not pursue this approach further here, which has merit when considering other aspects of hadronic spectra.

Using the SU(2) flavor exchange operator we find that the chromo-magnetic interaction term of light quarks u, d assumes the form:

$$\mu_I^{hl} = \frac{n_l(n_l-6)}{12} + \frac{1}{4} I(I+1) + \frac{1}{12} S_l(S_l+1) + \frac{1}{4} C_2^l(p, q). \quad (26)$$

where the index *light* reminds us that here we have only accounted for the light quark u, d contribution and quantum numbers in all hadrons. In deriving Eq. (26) we have used some well known relations:

$$\begin{aligned} 2 \sum_{i>j} I^i \cdot I^j &= \left(\sum_i I^i \right) \cdot \left(\sum_j I^j \right) - \sum_i (I^i)^2, \\ 2 \sum_{i>j} S^i \cdot S^j &= \left(\sum_i S^i \right) \cdot \left(\sum_j S^j \right) - \sum_i (S^i)^2 \\ 2 \sum_{i>j} \lambda^i \cdot \lambda^j &= \left(\sum_i \lambda^i \right) \cdot \left(\sum_j \lambda^j \right) - \sum_i \lambda^i \cdot \lambda^i \end{aligned}$$

and

$$\left(\sum_i I^i\right)^2|h\rangle = I(I+1)|h\rangle, \quad \left(\sum_i s^i\right)^2|h\rangle = S(S+1)|h\rangle.$$

given the total spin and isospin operators introduced implicitly above. Everything works in the same way for the color group $SU(3)$, except that the individual quadratic Casimir operator has a different eigenvalue to keep in mind. In the fundamental representation

$$C_2(\underline{\mathbf{3}}) \equiv \sum_{a=1}^8 \left(\frac{\lambda_a^i}{2}\right)^2 = \frac{4}{3},$$

which is just the inverse of $3/4$, the eigenvalue of the quadratic Casimir operator for the $SU(2)$ in the fundamental representation $\underline{\mathbf{2}}$. For the composite state $|h\rangle$ of particles q and antiparticles \bar{q} in fundamental representation we have:

$$\sum_{a=1}^8 \left(\sum_i \frac{\lambda_a^i}{2}\right)^2 |h\rangle = C_2(p, q)|h\rangle,$$

where the values of (p, q) for a few representations are: $\underline{\mathbf{1}}=(0,0)$, $\underline{\mathbf{3}}=(0,1)$, $\underline{\mathbf{3}}=(1,0)$, $\underline{\mathbf{6}}=(2,0)$, $\underline{\mathbf{6}}=(0,2)$, $\underline{\mathbf{8}}=(1,1)$, $\underline{\mathbf{10}}=(3,0)$, etc. More generally, the dimension of the representation and the Young-tableaux numbers p, q are related by:

$$d(p, q) = \frac{1}{2}(p+1)(q+1)(p+q+2).$$

The quadratic Casimir operator in terms of p, q assumes the values

$$C_2(p, q) = p + q + \frac{p^2}{3} + \frac{pq}{3} + \frac{q^2}{3}.$$

Explicitly:

$$C_2(\underline{\mathbf{1}}) = 0, \quad C_2(\underline{\mathbf{3}}) = C_2(\underline{\mathbf{3}}) = \frac{4}{3}, \quad C_2(\underline{\mathbf{6}}) = C_2(\underline{\mathbf{6}}) = 3\frac{1}{3}, \quad C_2(\underline{\mathbf{8}}) = 3.$$

It is with great satisfactions that we note that Eq.(26) has a minimum for $n_l = 3$, corresponding to the baryon system, and that overall the chromo-magnetic interaction energy factor is negative only for the nucleon state among the three quark states. The splitting of N and Δ (difference between $I = 3/2, S = 3/2$ and $I = 1/2, S = 1/2$ states) $M_\Delta - M_N = \delta E$ thus leads to^a

^a When fitting the mass of the Δ one has to note that the coupling to a strong decay channel also shifts the quark based hadron mass downward yielding the physical mass, and hence the quark-based portion of the Δ mass is to be taken at $M_\Delta + \Gamma_\Delta$

$\delta E \simeq -400\text{MeV}$, which is consistent with the splitting $M_\Sigma - M_\Lambda = (3/16) \delta E$ (difference between $I = 0$ and $I = 1$ states).

These are very persuasive examples of the successes of the bag model of quark structure of hadrons, and prove that the hadron masses are properly described by the color magnetic interaction.

Limitations of the quark-bag picture

But if Eq. (20) works very well for the fundamental multiplets of baryons and mesons, why is it that it also predicts unwanted states such as baryonium $qq\bar{q}\bar{q}$, the $qq\bar{s}\bar{q}\bar{s}$ di-baryons and many more, not seen? Some of these exotica are quite stable: which multi-quark states are most bound can be deduced from the general bonding (Hund) rule of quark physics³⁵:

- the quarks and antiquarks are separately in the largest possible representation of color and spin, and
- the total state is in the smallest possible representation of spin and color.

Thus the state with the structure $[(uds)_{8_c, 4_s} \otimes (uds)_{8_c, 4_s}]_{0_c, 0_s}$ where the sub-indices refer to color and spin multiplicities of the representations is the most bound exotic 6 quark state. Such a hadron has not been found despite literally twenty different experimental searches. So probably not all is well with our current understanding of quark structure in hadrons and strong interactions. It could be that the small size of normal hadrons may not yet require a fully dissolved vacuum structure, while the larger exotica do require full structure dissolution. In such a case there is additional vacuum energy cost required to form these larger exotic states, a fact which would induce considerable instability by hadronic dissociation. The hope is that the study of really large chunks of quark matter we call quark-gluon plasma will provide a shortcut to a resolution of this problem.

Let us hence make a step back and look again at the hadron structure fit³² – if this fit is so successful, what does it tell us about the volume energy, which is the ‘condensation’ latent energy of the vacuum? The fitted value $\mathcal{B}_b^{1/4} = 170 \text{ MeV}$, which we also can express as $\mathcal{B}_b = 0.1\text{Gev}/\text{fm}^3$ is relatively small. The magnitude derives from the fact that the quark-related energy component in the hadron is 3/4 of the total, as can be seen solely on dimensional grounds inspecting Eqs. (18,19), since only terms changing with R as R^3 and $1/R$ appear. The volume energy component in the nucleon is thus about $m/4 = 235 \equiv \mathcal{B}_b V_h \text{ MeV}$. Only if we could make hadron volume V_h very small, the volume energy could come out big. However the elastic electromagnetic form factors and other electromagnetic properties of hadrons indicate that the

Maxwell-charge distribution inside hadron is not less than 0.7–0.8 fm in size. The above considered value of the volume energy leads to a quark confinement volume with radius $R = 0.83$ fm, for protons, compared with the charge radius $\langle r^2 \rangle = (0.86 \text{ fm})^2$. Clearly, there is not much room for change and surely we will not be able to find $\mathcal{B} = \mathcal{O}(1) \text{ GeV/fm}^3$, a value motivated by numerical simulations of lattice QCD⁵.

3 Quark-Gluon Plasma

Relativistic heavy ion experiments

In order to form relatively large quark-gluon filled space-time regions the best tool we have today are large nuclei. These nuclei are made to collide at very high energies, many times higher than the rest mass of particles involved. The relativistic energy is required to produce regions of space filled with movable color charges of quarks and gluons, the quark-gluon plasma (QGP). Primarily because the identification of this new, locally deconfined form of matter is difficult, the object we search for seems to be the never-to-be-found nuclear Holy Grail. However, this deconfined QGP state must in principle exist if QCD is the true theory of strong interactions: such a free quark-gluon phase is clearly seen in numerical studies of QCD within the lattice gauge theory (LGT) simulations, though the details of the quark structure of the deconfined state remain today somewhat obscured by the difficulties that one encounters in numerical treatment of Fermions⁵.

The study of highly excited and dense hadronic matter by means of ultra-relativistic nuclear collisions is a relatively novel, interdisciplinary area of research in rapid experimental and theoretical evolution. It is closely related to the fields of nuclear and particle physics and, accordingly, our material encompasses aspects of both these wide research areas. Among ‘consumers’ of the material presented here we also encounter researchers in the fields of astrophysics and cosmology. The idea to test this is to squeeze and compress large nuclei, such that individual nucleons are made to fuse into a new common structure comprising freely moving quarks.

The initial experimental programs were launched nearly 30 years ago at the Lawrence Berkeley Laboratory (LBL) at Berkeley, USA, and at the Dubna Laboratory (Russia) for lighter ions. Another 1-2 GeV facility, SIS, of comparable physics perspective has come on line in recent years at GSI in Darmstadt, Germany. A greater beam intensity and new detector technologies at SIS allow to explore systematically phenomena that could not be studied at the BEVALAC. Studies of properties of excited nuclear matter performed at these facilities display particle spectra ‘temperatures’ of the order of 100 MeV,

accompanied by relatively abundant pion production.

These first advances were made with relatively modest energies, and the results had mainly bearing on the properties of the nuclear matter close to the conditions encountered in supernova explosions. However, they demonstrated the possibility to study the properties of compressed and excited nuclear matter in laboratory. Together with the theoretical work, these results implied that QGP could be in reach of existing accelerator facilities. Thus a search for the point of transition from the hadronic gas phase of locally confined nucleons, mesons, etc, to the deconfined QGP phase that gave birth to the development of the present day research program, in USA at BNL (Brookhaven National Laboratory, Upton – Long Island, New York), and in Europe at CERN (European Nuclear Physics Research Laboratory, Geneva). The first Oxygen beam at 60 A GeV was extracted from the SPS (Super Proton Synchrotron) accelerator at CERN and met target in the late fall of 1986, about the same time as BNL started its experimental program at AGS (Alternate Gradient Synchrotron) accelerator with 15 A GeV Silicon ions. Very soon after, the energy of the SPS beam could be increased to 200 A GeV and a Sulphur ion source was added. In order to allow experiments to study the relatively large volumes and longer lifetimes expected in dense matter formed in collision of heaviest nuclei, an upgrade of SPS injection system was carried out, which allowed to accelerate the Lead ions to 158 A GeV in the Fall of 1994. At BNL, a similar development allowed to accelerate Gold beams to 11 A GeV at the AGS.

Today we are repositioning our interests around two new experimental facilities: RHIC and LHC. The RHIC (Relativistic Heavy Ion Collider) at BNL, is slated for physics progress in 1999, with colliding nuclear beams at up to 100 A GeV, thus allowing exploration of a entirely new domain of energy, 10 times greater than currently available at SPS. The LHC (Large Hadron Collider) which is being developed at CERN, should be commissioned at midpoint of the first decade of XXI century, and it will devote an important part of its beam time to the acceleration of nuclear beams. The final energy available at the LHC is expected to be a factor 30 or more higher compared to RHIC.

Many experiments are in progress both at CERN and BNL and our present interest addresses primarily results obtained at the higher CERN energies, involving strange particle production. Several experiments comprise similar ‘crews’ and we will group their names together. This leaves us with two major lines of approach: NA35/NA49 and WA85/WA94/WA97/NA57. While the NA35 etc groups are interested in obtaining full phase space coverage and use detectors such as streamer chambers and time projection chambers, the WA85 etc groups concentrate on a small window of phase space ‘opportunity’ with

a spectrometer, which allows to identify and observe rarely produced multi-strange particles. Another series of experiments which is of some importance for our study of heavy flavor quarks is NA38/NA50/NA51 series, which observes by means of their dimuon decays the production of vector mesons.

The first conclusion one can draw from the recent results including the collisions of Pb–Pb nuclei involving projectiles colliding with a laboratory fixed target at 158 A GeV is that there is a localized space-time region in which high concentration of matter and energy is reached: we refer to this object as ‘fireball’. We believe that local thermal equilibrium is established within the volume occupied by the fireball, and thus particles emerge with spectra characteristic of the surface temperature and velocity.

Probes of dense hadronic matter

Since in the collision of large nuclei, the highly dense state is formed for a rather short time of magnitude $2R/c$, where R is the nuclear radius, one of the major challenges has been to identify suitable physical observable of deconfinement. This difficult problem of detecting reliably the formation of an unknown phase of matter, existing only as short as $0.5 \cdot 10^{-22}$ sec, has not been completely resolved today. The electromagnetic probes involving directly produced photons and dileptons are witnesses to the earliest moments of the reaction, but their production rates are in general very small, the experimental γ yield is dominated by the secondary processes $\pi^0 \rightarrow \gamma + \gamma$. The dilepton yield is also mostly resulting from meson decays, but there are small kinematic regions where this background yield is very small. Moreover, the dilepton spectrum gives interesting insights about the vector meson yields and their variation with experimental conditions. We will briefly address here this very interesting observable.

The principal observable of the relativistic nuclear collision process are spectra of hadronic (strongly interacting) particles. Their multiplicity is growing rapidly with both energy and size of the projectile-target nuclei. Aside of the single particle spectra one can also relatively easily measure two particle correlations. The HBT correlation measurement is widely used to determine the geometric properties of the central fireball, and the results agree with a reaction picture between the nuclei relying on geometric considerations. However, this approach is still plagued by fundamental and unresolved issues. Work is progressing rapidly in this field and which is addressed in full in this volume by Baym and Heinz³⁶.

Strangeness³⁷ (and at RHIC/LHC also charm) and entropy³⁸ are good hadronic observable since both will be preserved by ‘reasonable’ evolution sce-

narios of the dense matter fireball: the melted QGP state is in general entropy richer than the frozen HG phase. Once entropy has been generated, it cannot be lost, an entropy excess accompanies QGP formation. When abundant particle production is possible, this entropy excess is seen as an enhancement in the total hadronic particle multiplicity with each (relativistic) meson carrying about 4 units of entropy out of the interaction region. Similarly, strangeness is in general more abundant in QGP than HG phase³⁷, and it is not re-annihilated in rapid decomposition of the dense matter state³⁹. It has become a key diagnostic tool of dense hadronic matter because:

1) particles containing strangeness are produced more abundantly in relativistic nuclear collisions than it could be expected based on simple scaling of p - p reactions;

2) all strange quarks have to be made, while light u , d quarks are also brought into the reaction by the colliding nuclei;

3) because there are many different strange particles, we have a very rich field of observable with which it is possible to explore diverse properties of the source;

4) theoretical calculations suggest that glue–glue collisions in the QGP provide a sufficiently fast and thus by far, a unique mechanism leading to an explanation of strangeness enhancement.

There are two generic flavor observable (strangeness and charm) which we study analyzing experimental data, and we introduce these here, without an effort to ‘orthogonalized’, *i.e.*, make them independent of each other:

- absolute yield of strangeness/charm
Once produced in hot and dense hadronic matter, *e.g.*, the QGP phase, strangeness/charm is not re-annihilated in the evolution of the deconfined state towards freeze-out, because in the expansion and/or cooling process the rate of production/annihilation rapidly diminishes and becomes negligible. Therefore the flavor yield is characteristic of the initial, most extreme conditions.
- phase space occupancy γ_i
 γ_i describes how close the flavor yield per unit of volume ($i = u, d, s$, and in some cases charm $i = c$ occupancy will be also considered) comes to the chemical equilibrium expected; γ_i impacts strongly the distribution of flavor among final state hadronic particles.

Because of the high density of the QGP phase, the phase space occupancy γ_i can saturate rapidly, and thus particle abundances will emerge from a chemically equilibrated u, d, s phase, which is hardly imaginable for conventional

reaction mechanisms. Because entropy and strangeness are enhanced in a similar way in QGP, the specific yield of strangeness per particle produced is not a good quantity to use when searching for the deconfined state. Many other strategies are available, of which we favor measurement of the specific entropy yield per participating baryon, accompanied by a study of relative strange antibaryon yields, involving particle ratios such as $\bar{\Lambda}/\bar{p}$ ³⁷. It is remarkable that the pertinent results obtained for S–Pb collisions by the NA35 collaboration⁴⁰ have shown the QGP related enhancement.

Recent results on strangeness

The possibility that strange particle anomalies seen in recent years at SPS in Sulphur induced reactions on heavy nuclei are arising in consequence to the formation of a deconfined QGP phase has stimulated the intense continuation of the experimental research program in the considerably more difficult, high particle multiplicity environment arising in Pb induced reactions, which are presently possible at 158A GeV.

The experiment WA97⁴¹ has further reported several specific strange baryon and antibaryon ratios from Pb–Pb collisions at 158A GeV, comprising 30% of inelastic interactions. All ratios are obtained in an overlapping kinematic window corresponding effectively to transverse momentum $p_{\perp} > 0.7$ GeV, within the central rapidity region $y \in y_{cm} \pm 0.5$. They have been corrected for weak interactions cascading decays. The experimental values are:

$$R_{\Lambda} = \frac{\bar{\Lambda}}{\Lambda} = 0.14 \pm 0.03, \quad R_{\Xi} = \frac{\bar{\Xi}}{\Xi} = 0.27 \pm 0.0, \quad R_{\Omega} = \frac{\bar{\Omega}}{\Omega} = 0.42 \pm 0.12, \quad (27)$$

$$R_s^p = \frac{\bar{s}}{s} = 0.14 \pm 0.02, \quad R_{\bar{s}}^p = \frac{\bar{\bar{s}}}{\bar{s}} = 0.26 \pm 0.05, \quad (28)$$

$$R_s^{\prime p} = \frac{\Omega}{\Xi} = 0.19 \pm 0.04, \quad R_{\bar{s}}^{\prime p} = \frac{\bar{\Omega}}{\bar{\Xi}} = 0.30 \pm 0.09. \quad (29)$$

Here, the lower index s, resp. \bar{s} , reminds us that the ratio measures the density of strange, resp. anti-strange, quarks relatively to light quarks. The upper index p indicates that the ratio is taken within a common interval of transverse momenta (and not common transverse mass). We compare R_s^p , $R_{\bar{s}}^p$ results with earlier measurements in Fig.1. The strange antibaryon enhancement effect is re-confirmed in the Pb–Pb data, and we see that there is no major change of this result, which determines the phase space occupancy of strangeness, as we move from S–S or S–W/Pb results to Pb–Pb results. There is agreement between WA97 and NA49 on the value of R_{Λ} , even though the data sample

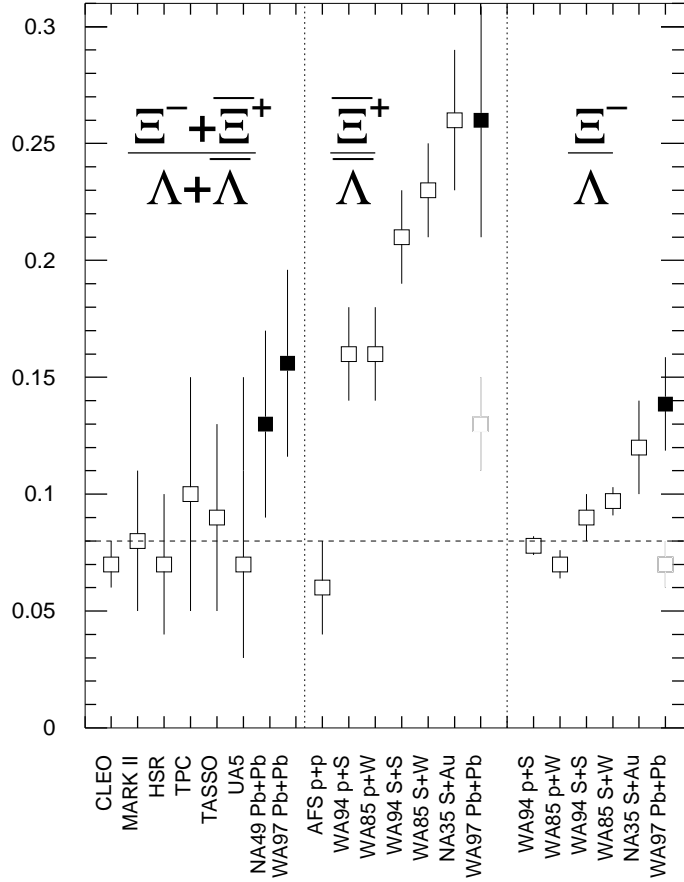


Figure 1: Sample of World results (as ‘function’ of experiment name for yields involving ratio of strange to non-strange quarks in baryons. Dark squares: recent Pb–Pb results.

of NA49 is taken for more central trigger, constrained to as few as 4% of most central collisions. The cuts in p_{\perp} and y are nearly identical in both experiments. From Fig. 3 in ⁴², we obtain the value $R_{\Lambda} = 0.17 \pm 0.03$, which we shall combine with the value given by WA97 and we thus take in our data fit:

$$R_{\Lambda} = \frac{\bar{\Lambda}}{\Lambda} = 0.155 \pm 0.04. \quad (30)$$

4 Strangeness Production

The coupling constant of strong interactions

The observed strange particles are presumably born in a deconfined phase which can make strange quark pairs effectively. It turns out that the production of strangeness is originating primarily in gluon-gluon collisions. We use two particle collision processes to evaluate thermal flavor production in QGP, as described in ⁶. However, since this report we have realized ^{46,47} that recent precise measurements of the strong interaction coupling constant α_s allow us to eliminate a lot of arbitrariness from the earlier calculations regarding the strength of the collision cross sections. The experimental measurements of α_s occurred at the scale of the the Z_0 mass, thus 92 GeV, and hence one has to use the powers of the renormalization group of QCD to evolve these results towards the here relevant domain. In the process we also allow for the evolution of the strange quark mass, which is also significant and is driven by the evolution of the coupling constant. We will now briefly explain how this is accomplished.

To determine the two QCD parameters required, we will use the renormalization group functions β and γ_m :

$$\mu \frac{\partial \alpha_s}{\partial \mu} = \beta(\alpha_s(\mu)), \quad \mu \frac{\partial m}{\partial \mu} = -m \gamma_m(\alpha_s(\mu)). \quad (31)$$

For our present study we will use the perturbative power expansion in α_s :

$$\beta^{\text{pert}} = \alpha_s^2 [b_0 + b_1 \alpha_s + \dots], \quad \gamma_m^{\text{pert}} = \alpha_s [c_0 + c_1 \alpha_s + \dots], \quad (32)$$

For the SU(3)-gauge theory with n_f Fermions the first two terms (two ‘loop’ order) are renormalization scheme independent, the three loop level b_2 is known in both MS (minimal subtraction) and $\overline{\text{MS}}$ (modified minimal subtraction) renormalization schemes ^{43,44}, while c_2 , so far we could ascertain, was only derived in the MS scheme. In any case we will restrict our study to the two loop order which does not require renormalization scheme improvements of the form of the two body cross sections. To this order we have:

$$b_0 = \frac{1}{2\pi} \left(11 - \frac{2}{3} n_f \right), \quad b_1 = \frac{1}{4\pi^2} \left(51 - \frac{19}{3} n_f \right), \quad (33)$$

$$c_0 = \frac{2}{\pi}, \quad c_1 = \frac{1}{12\pi^2} \left(101 - \frac{10}{3} n_f \right). \quad (34)$$

The number n_f of Fermions that can be excited, depends on the energy scale μ . We have implemented this using the exact phase space form appro-

appropriate for the terms linear in n_f

$$n_f(\mu) = 2 + \sum_{i=s,c,b,t} \sqrt{1 - \frac{4m_i^2}{\mu^2}} \left(1 + \frac{2m_i^2}{\mu}\right) \Theta(\mu - 2m_i), \quad (35)$$

with $m_s = 0.16$ GeV, $m_c = 1.5$ GeV, $m_b = 4.8$ GeV. We checked that there is very minimal impact of the running of the masses in Eq. (35) on the final result, and will therefore not introduce that ‘feed-back’ effect into our current discussion. The largest influence on our solutions comes here from the bottom mass, since any error made at about 5 GeV is amplified most. However, we find that this results in a scarcely visible change even when the mass is changed by 10% and thus one can conclude that the exact values of the masses and the nature of flavor threshold is at present of minor importance in our study. We show the result of numerical integration for α_s in the top portion of Fig. 2. First equation in (31) is numerically integrated beginning with an initial value of $\alpha_s(M_Z)$. We use in this report the August 1996 World average⁴⁵: $\alpha_s(M_Z) = 0.118$ for which the estimated error is ± 0.003 . This value is sufficiently precise to reduce this uncertainty below that has limited our earlier study⁴⁶. In addition, the thin solid lines present results for $\alpha_s(M_Z) = 0.115$ till recently the preferred result in some analysis, especially those at lower energy scale. As seen in Fig. 2, the variation of α_s with the energy scale is substantial, and in particular we note the rapid change at and below $\mu = 1$ GeV, where the strange quark flavor formation occurs in hot QGP phase formed in present day experiments at 160–200 A GeV (SPS-CERN). Clearly, use of constant value of α_s is hardly justified, and the first order approximation often used:

$$\alpha_s(\mu) \equiv \frac{2b_0^{-1}(n_f)}{\ln(\mu/\Lambda_0(\mu))^2}, \quad (36)$$

can be seen to be not a good approximation till rather high $\mu = 50$ GeV scale is reached: we insert the numerically computed value of α_s into Eq. (36) and obtain $\Lambda_0(\mu)$ which would yield the given $\alpha_s(\mu)$. This procedure leads to a strongly scale dependent $\Lambda_0(\mu)$ shown in the middle section of Fig. 2.

Given $\alpha_s(\mu)$, we can integrate the running of the quark masses, the second equation in (31). Because the running mass equation is linear in m , it is possible to determine the universal quark mass scale factor

$$m_r = m(\mu)/m(\mu_0). \quad (37)$$

Since α_s refers to the scale of $\mu_0 = M_Z$, it is a convenient reference point also for quark masses. As seen in the bottom portion of Fig. 2, the change in the quark

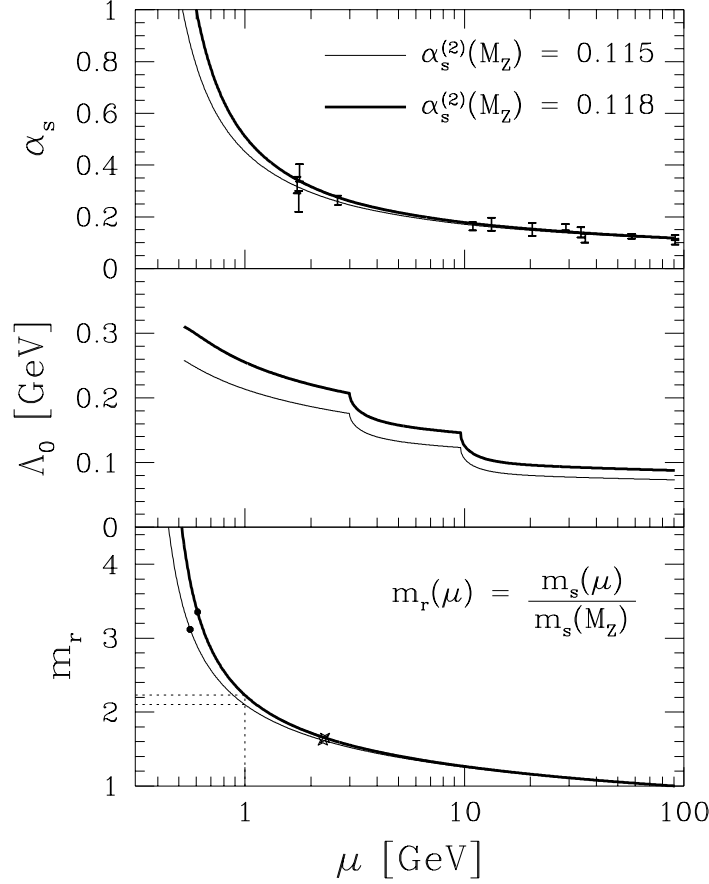


Figure 2: $\alpha_s(\mu)$ (top section); the equivalent parameter Λ_0 (middle section) and $m_r(\mu) = m(\mu)/m(M_Z)$ (bottom section) as function of energy scale μ . Initial value $\alpha_s(M_Z) = 0.118$ (thick solid lines) and $\alpha_s(M_Z) = 0.115$ (thin solid lines). In lower section the dots indicate the strangeness pair production thresholds for $m_s(M_Z) = 90$ MeV, while crosses indicate charm pair production thresholds for $m_c(M_Z) = 700$ MeV.

mass factor is highly relevant in the study of strangeness and charm production, since it is driven by the rapidly changing α_s near to $\mu \simeq 1$ GeV. For each of the different functional dependencies $\alpha_s(\mu)$ we obtain a different function m_r . The significance of the running of the charmed quark mass cannot be stressed enough, especially for thermal charm production occurring in foreseeable future

experiments well below threshold, which makes the use the exact value of m_c necessary.

Given these results, we find that for $\alpha_s = 0.118$ and $m_s(M_Z) = 90 \pm 18$ MeV a low energy strange quark mass $m_s(1 \text{ GeV}) \simeq 200 \pm 40$ MeV, in the middle of the standard range $100 < m_s(1 \text{ GeV}) < 300$ MeV. Similarly we consider $m_c(M_Z) = 700 \pm 50$ MeV, for which value we find the low energy mass $m_c(1 \text{ GeV}) \simeq 1550 \pm 110$ MeV, at the upper (conservative for particle production yield) end of the standard range $1 < m_c(1 \text{ GeV}) < 1.6$ GeV. The energy threshold for pair production E_i^{th} , $i = s, c$, has to be determined in a separate calculation since it is related to the scale of energy required for the production of two zero momentum particles $E_{\text{th}} = 2m(\mu = E_{\text{th}})$, and thus:

$$E_i^{\text{th}} = 2m_i(M_Z)m_r(E_i^{\text{th}}). \quad (38)$$

This effect stabilizes strangeness production cross section in the infrared: below $\sqrt{s} = 1$ GeV the strange quark mass increases rapidly and the threshold mass is considerably greater than $m_s(1 \text{ GeV})$. We obtain the threshold values $E_s^{\text{th}} = 605$ MeV for $\alpha_s(M_Z) = 0.118$ and $E_s^{\text{th}} = 560$ MeV for $\alpha_s(M_Z) = 0.115$. Both values are indicated by the black dots in Fig. 2. For charm, the running mass effect has the opposite effect: since the mass of charmed quarks is listed in tables for $\mu = 1$ GeV, but the here explored value of the mass is above 1 GeV, the charm production threshold turns out to be smaller than expected. There is little uncertainty with regarding the coupling constant; for $m_c(M_Z) = 700$ MeV the production threshold is found at $E_c^{\text{th}} \simeq 2.3$ GeV rather than $2 \cdot 1.55 = 3.1$ GeV, the value we would have obtained using $m_c(1 \text{ GeV})$ in this case. This reduction in threshold energy enhances strongly the thermal production of charm at ‘low’ temperatures $T \simeq 250$ MeV, where it is suppressed exponentially by a factor $\propto \exp(-E^{\text{th}}/T)$.

QCD strangeness production processes

The generic angle averaged two particle cross sections for (heavy) flavor production processes $g + g \rightarrow f + \bar{f}$ and $q + \bar{q} \rightarrow f + \bar{f}$, are among classic results of QCD and are given by

$$\bar{\sigma}_{gg \rightarrow f\bar{f}}(s) = \frac{2\pi\alpha_s^2}{3s} \left[\left(1 + \frac{4m_f^2}{s} + \frac{m_f^4}{s^2} \right) \tanh^{-1}W(s) - \left(\frac{7}{8} + \frac{31m_f^2}{8s} \right) W(s) \right], \quad (39)$$

$$\bar{\sigma}_{q\bar{q} \rightarrow f\bar{f}}(s) = \frac{8\pi\alpha_s^2}{27s} \left(1 + \frac{2m_f^2}{s} \right) W(s), \quad (40)$$

where $W(s) = \sqrt{1 - 4m_f^2/s}$, and both the QCD coupling constant α_s and flavor quark mass m_f will be in this work the running QCD parameters. In this way a large number of even- α_s diagrams contributing to flavor production is accounted for.

Other processes in which at least one additional gluon is present are not within the present calculational scheme. While only in very high density environment we could imagine relevant contributions from three body initial state collisions, emission of one or even several soft gluons in the final state could be relevant, thus this subject area will be surely revisited in the future. We note that a process in which a massive ‘gluon’, that is a quasi-particle with quantum numbers of a gluon, decays into a strange quark pair, is partially included in our work. At the present time we do not see a systematic way to incorporate any residue of this and other effects, originating in matter surrounding the microscopic processes, as work leading to understanding of renormalization group equations in matter (that is renormalization group at finite temperature and/or chemical potential) is still in progress ⁴⁸.

The master equation for flavor production, allowing for the detailed balance reactions, thus re-annihilation of flavor, is:

$$\frac{dN_i(t)}{dt} = V(t)A_i [1 - \gamma_i^2(t)] . \quad (41)$$

where A_i is the invariant rate per unit volume and time, that is the thermal average of the production cross section:

$$\begin{aligned} A_i &\equiv A_{gg} + A_{u\bar{u}} + A_{d\bar{d}} + \dots \\ &= \int_{4m_i^2}^{\infty} ds 2s \delta(s - (p_1 + p_2)^2) \int \frac{d^3 p_1}{2(2\pi)^3 E_1} \int \frac{d^3 p_2}{2(2\pi)^3 E_2} \\ &\quad \times \left[\frac{1}{2} g_g^2 f_g(p_1) f_g(p_2) \bar{\sigma}_{gg}(s) + n_f g_q^2 f_q(p_1) f_{\bar{q}}(p_2) \bar{\sigma}_{q\bar{q}}(s) + \dots \right] \end{aligned} \quad (42)$$

The dots indicate that other mechanisms may contribute to flavor production. The particle distributions f are in our case thermal Bose/Fermi functions, and $g_q = 6$, $g_g = 16$. For strangeness production $n_f = 2$, and for charm production $n_f = 3$, will be used.

We introduce also the flavor production relaxation time constant:

$$\tau_i \equiv \frac{1}{2} \frac{\rho_i^{\infty}(\tilde{m}_i)}{(A_{gg} + A_{qq} + \dots)} . \quad (43)$$

Here \tilde{m}_i is the mass at the scale of energy under study; we recall that the equilibrium distribution is result of Boltzmann equation description of two

body collisions. Thus the mass arising in the equilibrium density ρ_i^∞ in Eq. (43) is to be taken at the energy scale of the average two parton collision. We adopt for strangeness a fixed value $\tilde{m}_s = 200$ MeV, and also $\tilde{m}_c = 1,500$ MeV, and observe that in the range of temperatures here considered the precise value of the strange quark mass is insignificant, since the quark density is primarily governed by the T^3 term in this limit, with finite mass correction being $\mathcal{O}(10\%)$. The situation is less clear for charm relaxation, since the running of the mass should have a significant impact.

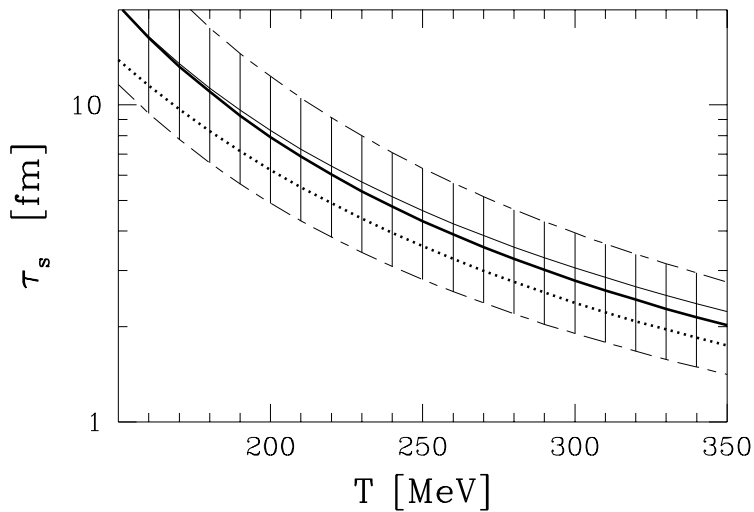


Figure 3: QGP strangeness relaxation time, for $\alpha_s(M_Z) = 0.118$, (thick line) and $= 0.115$ (thin line); $m_s(M_Z) = 90$ MeV. Hatched areas: effect of variation of strange quark mass by 20%. Dotted: comparison results for fixed $\alpha_s = 0.5$ and $m_s = 200$ MeV.

We can now proceed to evaluate the relaxation times for strangeness and charm production. The current calculation offers an upper limit on the actual relaxation time, which may still be smaller, considering that other mechanisms may contribute to flavor production, as is shown by the dots in Eq. (42). We show in Fig. 3 also the impact of a 20% uncertainty in $m_s(M_Z)$, indicated by the hatched areas. This uncertainty is today much larger compared to the uncertainty that arises from the recently improved precision of the strong coupling constant determination⁴⁵. We note that the calculations made at fixed values $\alpha_s = 0.5$ and $m_s = 200$ MeV (dotted line in Fig. 3) are well within the band of values related to the uncertainty in the strange quark mass.

Since charm is somewhat more massive compared to strangeness, there

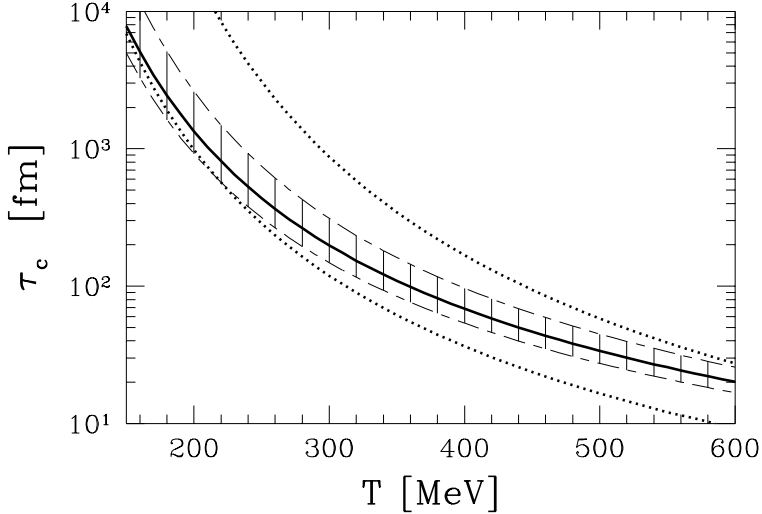


Figure 4: Solid lines: thermal charm relaxation constant in QGP, calculated for running $\alpha_s(M_Z) = 0.115; 0.118$, (indistinguishable), $m_c(M_Z) = 700$ MeV. Lower dotted line: for fixed $m_c = 1.1$ GeV, $\alpha_s = 0.35$; upper dotted line: for fixed $m_c = 1.5$ GeV, $\alpha_s = 0.4$. Hatched area: effect of variation $m_c(M_Z) = 700 \pm 50$ MeV.

is still less uncertainty arising in the extrapolation of the coupling constant. Also the systematic uncertainty related to the soft gluons (odd- α_s) terms are smaller, and thus the relaxation times τ_c we show in Fig.4 are considerably better defined compared to τ_s . There is also less relative uncertainty in the value of charm mass. We also show in Fig.4 (dotted lines) the fixed m_c, α_s results with parameters selected to border high and low T limits of the results presented. It is difficult to find a good comparative behavior of τ_c using just one set of m_c and α_s . This may be attributed to the importance of the mass of the charmed quarks, considering that the threshold for charm production is well above the average thermal collision energy, which results in emphasis of the effect of running charm mass. In the high T -limit the choice (upper dotted line in Fig.4) $m_c = 1.5$ GeV, $\alpha_s = 0.4$ is appropriate, while to follow the result at small T (lower dotted line in Fig.3) we take a much smaller mass $m_c = 1.1$ GeV, $\alpha_s = 0.35$.

Temporal evolution of the fireball

In order to compute the production and evolution of strangeness (and charm) flavor a more specific picture of the temporal evolution of dense matter is needed. In a simple, qualitative description, we assume that the hot, dense matter is homogeneous. We consider that, in Pb–Pb collisions at SPS, the radial expansion is the dominant factor for the evolution of the fireball properties such as temperature/energy density and lifetime of the QGP phase. The expansion dynamics follows from two assumptions:

- the (radial) expansion is entropy conserving, thus the volume and temperature satisfy

$$V \cdot T^3 = \text{Const.} \quad (44)$$

- the surface flow velocity is given by the sound velocity in a relativistic gas

$$v_f = 1/\sqrt{3}. \quad (45)$$

It is well understood that expansion into ‘vacuum’ of relativistic matter can proceed at any velocity, up to velocity of light. However, here v_f is understood not as the velocity of the first flow edge, it is the velocity of the flow of matter from interior of the fireball to the near surface region, which cannot exceed the speed of sound in the matter, unless a shock is created. We will return to this intricate issue in the near future⁴⁹.

These two assumption imply the following explicit forms for the radius of the fireball and its average temperature:

$$R = R_{\text{in}} + \frac{1}{\sqrt{3}}(t - t_{\text{in}}), \quad T = \frac{T_{\text{in}}}{1 + (t - t_{\text{in}})/\sqrt{3}R_{\text{in}}}. \quad (46)$$

We shall see below that if QGP formation is involved, a fit of strange antibaryons data either leads to direct emission before expansion, or to emission from a surface expanding with just this velocity v_f .

The initial conditions have been determined such that the energy per baryon is given by energy and baryon flow, and the total baryon number is $\eta(A_1 + A_2)$, as stopped in the interaction region. They are shown in table 2. The radius are for zero impact parameter. For this, equations of state of the QGP are needed, and we have employed our model⁵⁰ in which the perturbative correction to the number of degrees of freedom were incorporated along with thermal particle masses.

Allowing for dilution of the phase space density in expansion, we integrate⁶ a population equations describing the change in $\gamma_s(t)$:

$$\frac{d\gamma_s}{dt} = \left(\gamma_s \frac{\dot{T}m_s}{T^2} \frac{d}{dx} \ln x^2 K_2(x) + \frac{1}{2\tau_s} [1 - \gamma_s^2] \right). \quad (47)$$

Table 2: The initial conditions for S–Pb/W at 200A GeV and Pb–Pb at 158A GeV for different stopping values η .

	t_{in} [fm]	η	R_{in} [fm]	T_{in} [MeV]	λ_q
S–Pb/W	1	0.35	3.3	280	1.5
	1	0.50	3.7	280	1.5
Pb–Pb	1	0.50	4.5	320	1.6
	1	0.75	5.2	320	1.6

Table 3: γ_s and N_s/B in S–W at 200A GeV and Pb–Pb at 158A GeV for different stopping values of baryonic number and energy $\eta_B = \eta_E$; computed for strange quark mass $m_s(1\text{GeV}) = 200 \pm 40$ MeV, $\alpha_s(M_Z) = 0.118$.

E_{lab}	S–W at 200A GeV		Pb–Pb at 158A GeV	
$\eta_B = \eta_E$	0.35	0.5	0.5	0.75
γ_s	0.53 ± 0.14	0.65 ± 0.15	0.69 ± 0.15	0.76 ± 0.16
N_s/B	0.67 ± 0.16	0.70 ± 0.16	0.954 ± 0.20	0.950 ± 0.20

Here K_2 is a Bessel function and $x = m_s/T$. Note that even when $1 - \gamma_s^2 < 1$ we still can have a positive derivative of γ_s , since the first term on the right hand side of Eq. (47) is always positive, both \dot{T} and $d/dx(x^2 K_2)$ being always negative. This shows that dilution due to expansion effects in principle can make the value of γ_s rise above unity.

Given the relaxation constant $\tau_s(T(t))$, these equations can be integrated numerically, and we can obtain for the two currently explored experimental systems the values of the two observables, γ_s and N_s/B , which are given in table 3. There is a considerable uncertainty due to the unknown mass of strange quarks. However, since this is not a statistical but systematic uncertainty depending nearly alone on the value of the strange quark mass parameter, all the results presented will shift together. We note further that there seems to be very little dependence on the stopping fractions in the yield of strange quarks per baryon N_s/B . Thus if the expected increase in stopping is confirmed, we should also expect a small increase by 15% in specific strangeness yield.

5 Hadronization from Fireball

Fireball parameters

We next introduce all the model parameters used in the fit of the particle ratios, not all will be required in different discussions of the experimental data. For more details about the thermo-chemical parameters we refer to the extensive

discussion in the earlier study of S–S and S–W data ⁵¹. The key parameters are:

1) T_f : the formation/emission/freeze-out temperature, depending on the reaction model. T_f enters in the fit of abundance ratios of unlike particles presented within a fixed p_\perp interval. The temperature T_f can in first approximation be related to the observed high- m_\perp slope T_\perp by:

$$T_\perp \simeq T_f \frac{1 + v_\perp}{\sqrt{1 - v_\perp^2 - v_\parallel^2}}. \quad (48)$$

In the central rapidity region the longitudinal flow $v_\parallel \simeq 0$, in order to assure symmetry between projectile and target. Thus as long as $T_f < T_\perp$, we shall use Eq.(48) setting $v_\parallel = 0$ to estimate the transverse flow velocity v_\perp of the source.

2) λ_q : the light quark fugacity. We initially used in our fits both u , d -flavor fugacities λ_u and λ_d , but we saw that the results were equally adequate without allowing for up-down quark asymmetry, using the geometric average $\lambda_q = \sqrt{\lambda_u \lambda_d}$; moreover the fitted up-down quark fugacity asymmetry was found as expected in our earlier analytical studies ⁵².

3) λ_s : the strange quark fugacity. A source in which the carriers of s and \bar{s} quarks are symmetric this parameter should have the value $\lambda_s \simeq 1$, in general in a re-equilibrated hadronic matter the value of λ_s can be determined requiring strangeness conservation.

4) γ_s : the strange phase space occupancy. Due to rapid evolution of dense hadronic matter it is in general highly unlikely that the total abundance of strangeness can follow the rapid change in the conditions of the source, and thus in general the phase space will not be showing an overall abundance equilibrium corresponding to the momentary conditions.

5) R_C^s : in table 4 we note this parameter describing the relative off-equilibrium abundance of strange mesons and baryons, using thermal equilibrium abundance as reference.

Parameter R_C^s is needed, when we have constraint on the strangeness abundance and/or when we address the abundance of mesons since there is no a priori assurance that the relative production/emission strength of strange mesons and baryons should proceed according to relative strength expected from thermal equilibrium. Moreover, it is obvious that even if re-equilibration of particles in hadronic gas should occur, this parameter will not easily find its chemical equilibrium value $R_C^s = 1$ as we alluded to in section 1. However, due to reactions connecting strange with non-strange particles we expect $R_C^s = R_C$, where R_C is the same ratio for non-strange mesons and baryons,

using thermal abundance as reference. The value of $R_C > 1$ implies meson excess abundance per baryon, and thus excess specific entropy production, also expected in presence of color deconfinement³⁸.

The relative number of particles of same type emitted at a given instance by a hot source is obtained by noting that the probability to find all the j -components contained within the i -th emitted particle is

$$N_i \propto \gamma_s^k \prod_{j \in i} \lambda_j e^{-E_j/T}, \quad (49)$$

and we note that the total energy and fugacity of the particle is:

$$E_i = \sum_{j \in i} E_j, \quad \lambda_i = \prod_{j \in i} \lambda_j. \quad (50)$$

The strangeness occupancy γ_s enters Eq.(49) with power k , which equals the number of strange and anti-strange quarks in the hadron i . With $E_i = \sqrt{m_i^2 + p^2} = \sqrt{m_i^2 + p_\perp^2} \cosh y$ we integrate over the transverse momentum range as given by the experiment (here $p_\perp > 0.6$ GeV) taking central rapidity region $y \simeq 0$ to obtain the relative strengths of particles produced. We then allow all hadronic resonances to disintegrate in order to obtain the final relative multiplicity of ‘stable’ particles required to form the observed particle ratios. This approach allows to compute the relative strengths of strange (anti)baryons both in case of surface emission and equilibrium disintegration of a particle gas since the phase space occupancies are in both cases properly accounted for by Eq.(49). The transverse flow phenomena enter in a similar fashion into particles of comparable mass and are not expected to influence particle ratios. Finally we note that particles which are easily influenced by the medium, such as ϕ , require a greater effort than this simple model, and are also not explored in depth here.

We obtain the least square fit for the eight above reported (anti)baryon ratios. Our first approach is motivated by the reaction picture consisting of direct emission from the QGP deconfined fireball. The value of statistical parameters controlling the abundances are thus free of constraints arising in an equilibrated hadronic gas (HG) state⁵². The fitted thermal parameters are presented in the first line of table 4 along with the total χ^2 for the eight ratios. The fit is quite good, the error shown corresponds to the total accumulated error from 8 measurements; even if one argues that it involves 4 parameters to describe 5 truly independent quantities, the statistical significance is considerable, considering that 8 different measurements are included. Such a free fit does not know that we are expecting that the final state comprises a balance $\langle s - \bar{s} \rangle = 0$. In order to estimate what would be implied by strangeness

Table 4: Values of fitted statistical parameters within thermal model, for 158A GeV Pb–Pb strange particle production data. Superscript star ‘*’: a fixed input value for equilibrium hadronic gas; subscript ‘|c’: value is result of the imposed strangeness conservation constraint. χ^2 is the total relative square error of the fit for all data points used. First result line: direct emission QGP model, no meson to baryon ratio fit. Second line: same, but with strangeness conservation yielding λ_s , and R_C^s variable. Line three: as in line two, in addition the meson to baryon ratio Eq.(52) is fitted. Line four: hadronic gas fit including the ratio Eq.(52).

$T_f[MeV]$	λ_q	λ_s	γ_s	R_C^s	χ^2
272 ± 74	1.50 ± 0.07	1.14 ± 0.04	0.63 ± 0.10	—	1.0
272 ± 74	1.50 ± 0.08	$1.14 _c$	0.63 ± 0.10	4.21 ± 1.88	1.0
151 ± 10	1.54 ± 0.08	$1.13 _c$	0.91 ± 0.09	0.85 ± 0.22	1.5
155 ± 7	1.56 ± 0.09	$1.14 _c$	1*	1*	7.6

conservation constraint among emitted hadrons we present in second line of table 4 the result of a fit assuming that the value of λ_s is result of the conservation constraint $\langle s - \bar{s} \rangle = 0$, and allowing $R_C^s \neq 1$, for there should be no chemical equilibrium among the emitted strange mesons and strange baryons in a sudden and early QGP disintegration. The statistical error is found the same as in line 1, since this approach substitutes one parameter (λ_s) by another (R_C^s). The implication of this fit is that there must be either an excess of strange mesons or depletion of strange baryons compared to thermal equilibrium expectation, since as we recall $R_C^s = C_M^s/C_B^s$ with C_i being the yield of particles, normalized to one for thermal equilibrium yield. In any case we see that strange meson excess is required, which is consistent with excess of entropy production.

The errors seen in the two first lines of table 4 on the statistical parameters arise in part from strong correlations among them. In particular the very large error in T_f arise from strong (anti) correlation with γ_s : we find that a change in one of these parameters is associated with a change in the other at 80% level. Further information about the relation of T_f and γ_s may be garnered from theoretical considerations. We evaluate using our dynamical strangeness production model in QGP how the value of γ_s depends on the temperature of particle production T_f . The most important parameter in such a theoretical evaluation is the initial temperature at which the deconfined phase is created. As noted above, we estimated this temperature at $T_{in} = 320$ MeV⁵⁰. Further uncertainty of the calculation arises from the strange quark mass taken here to be $m_s(1\text{ GeV}) = 200$ MeV. We recall that the strength of the production rate is now sufficiently constrained by the measurement of $\alpha_s(M_Z)$. We choose a geometric size which comprises a baryon number $B = 300$ at $\lambda_q \simeq 1.5$, and

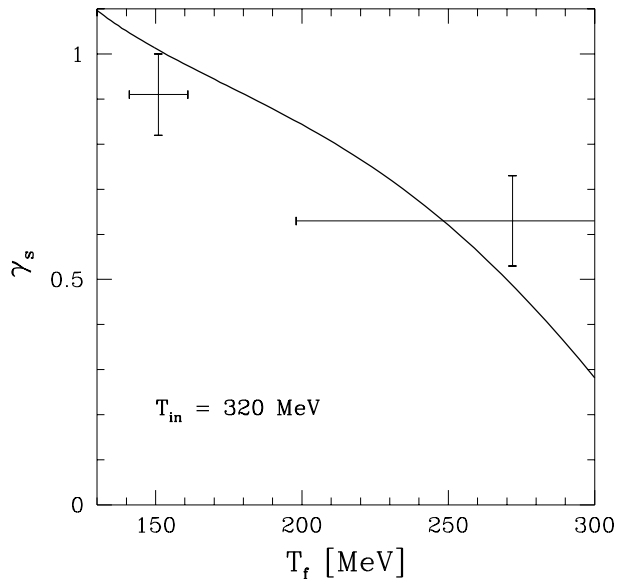


Figure 5: QGP strangeness occupancy γ_s as function of temperature T_f at time of particle production, for initial temperature $T_{in} = 320$ MeV, with $\gamma_s(T_{in}) = 0.1$.

have verified that our result will be little dependent on small variations in B . We show in Fig. 5 how the computed γ_s depends on formation temperature T_f . The cross to the right shows our fitted value from line 1 or 2 in table 4. It is gratifying to see that it is consistent with the theoretical expectation for early formation of the strange (anti)baryons. The relative smallness of γ_s , despite the high strangeness yield, is clearly related to the high temperature of particle production. We will below discuss the opposite scenario: the late freeze-out of strange particles.

The relatively high value of temperature T_f we obtained in the reaction picture with primordial particle emission is consistent with the experimental inverse slopes of the spectra. We are thus led to the conclusion that as far as the fitted temperatures and slopes are concerned, it is possible that the high m_\perp strange (anti)baryons we have described could have been emitted directly from a primordial (deconfined) phase before it evolves into final state hadrons.

We now consider at the experimental inverse m_\perp slopes. In the common p_\perp range of WA97 and NA49 experiments the transverse mass spectrum of Λ and $\bar{\Lambda}$

obtained by NA49 is very well describe by an exponential⁴². A thermal model motivated fit of the inverse slope (temperature) yields $T_{\perp}^{\Lambda} = 284 \pm 15$ MeV and $T_{\perp}^{\bar{\Lambda}} = 282 \pm 20$ MeV. This is consistent with the mid-rapidity proton and antiproton slope of the NA44 experiment: $T_p = 289 \pm 7$ MeV and $T_{\bar{p}} = 278 \pm 9$ MeV. For $\Xi + \bar{\Xi}$ a consistent value $T_{\Xi} = 290$ MeV is also quoted by the NA49–collaboration⁵³. We note that because the baryon masses are large, all these slopes are at relatively high $m_{\perp} > 1.3$ GeV (for nucleons, in NA44, $m_{\perp} > 1$ GeV). Systematically smaller inverse-transverse slopes are reported at smaller m_{\perp} , for kaons $T_{\perp}^K \simeq 213$ – 224 MeV for $0.7 < m_{\perp} < 1.6$ GeV in NA49⁴² and $T_{\perp}^{K^+} = 234 \pm 6$, $T_{\perp}^{K^-} = 235 \pm 7$ MeV in NA44⁵⁴; and 155–185 MeV for π ,^{42,54}, depending on the range of p_{\perp} , but here we have to remember that pions are known to arise primarily from resonance decays. An increase of T with m_{\perp} is most naturally associated with the effects of transverse flow of the source.

Is QGP primordial emission hypothesis also consistent with the chemical fugacities we have obtained? The chemical condition is fixed to about 5% precision, and there is 40% anti-correlation between the two fugacities λ_q and λ_s . The information that $\lambda_s \neq 1$ is contained in at least two particle abundances; arbitrary manipulation of the reported yields of one particle abundance did not reduce the value λ_s to unity. Since $\lambda_s \neq 1$ by 4 s.d. it is highly unlikely that $\lambda_s = 1$ is found after more data is studied. While one naively expects $\lambda_s^{\text{QGP}} = 1$, to assure the strangeness balance $\langle s - \bar{s} \rangle = 0$, there must be a small deviations from this value, even if the emitted particles were to reach asymptotic distances without any further interactions: in presence of baryon density the deconfined state is not fully symmetric under interchange of particles with antiparticles. A possible mechanism to distinguish the strange and anti-strange quarks arises akin to the effect considered for the K^-/K^+ asymmetry in baryonic matter^{55,56}: there is asymmetric scattering strength on baryon density ν_b which causes presence of a mean effective vector potential W . Similarly, strange quark interaction with baryon density would lead to a dispersion relation

$$E_{s/\bar{s}} = \sqrt{m_s^2 + p^2} \pm W, \quad (51)$$

and this requires in the statistical approach that the Fermi distribution for strange and anti-strange quarks acquires a compensating fugacity $\lambda_{s,\bar{s}} = e^{\pm W/T}$ to assure strangeness balance in the deconfined phase. In linear response approach $W \propto \nu_b$ consistent with both W and baryon density $\nu_b = (n_q - n_{\bar{q}})/3$, being fourth component of a Lorentz-vector. It is clear for intuitive reasons, as well as given experimental observations, that the baryon stopping and thus density increases considerably comparing the S and Pb induced reactions in the energy domain here considered. We also recall that in S–W reactions

$\lambda_s^S \simeq 1.03 \pm 0.05$ ⁵⁷. Should in the dense matter fireball the baryon density ν_b grow by factor 2–4 as the projectile changes from S to Pb, this alone would consistently explain the appearance of the value $\lambda_s = 1.14 \pm 0.04$ obtain using $W \propto \nu_b$ scaling. It is worth noting that the value $W \simeq 38 \text{ MeV}$ suffices here. Note also that the Coulomb potential effect on the charge of the strange quarks is of opposite magnitude and about 1/5–1/6 of the here required strength.

Late emission scenario: HG with or without QGP?

A generally favored picture of particle production involves flow expansion of the primordial phase till a transition temperature is reached, at which time the final state hadrons are produced, and soon thereafter freeze out. These particles may directly reach a detector or re-equilibrate and appear to the observer as if emitted from a HG phase, except that entropy/strangeness excess effect should remain. In order to force our data fit to converge to such a late particle production scenario we introduce the experimental result, which was essential for such an argument in the S–Pb induced reactions. The quantity of interest is ratio of particle yields between particles of very different mass. Thus in lines 3, 4 in table 4 we include in the fit also as experimental input an estimate of the hyperon to kaon ratio, thus altogether we now fit 9 data points.

We note that the NA49 spectra⁴² of kaons and hyperons have a slightly overlapping domain of m_\perp . We recall that the slopes are not exactly equal, thus all we can do is to try to combine the two shapes, assuming continuity consistent with flow, and to estimate the relative normalization of both that would place all experimental points on a common curve. We have carried out this procedure and obtained:

$$\left. \frac{\Lambda}{K_s^0} \right|_{m_\perp} \simeq 6.2 \pm 1.5. \quad (52)$$

Note that there is a tacit presumption in our approach that a similar effective Δy interval was used in both spectra. We recall that this ratio was 4.5 ± 0.2 in the S-W data⁵⁸.

Our approach in the third line corresponds to a freeze-out from ‘cold’ QGP phase, in that we allow the abundance parameters γ_s and R_C^S to deviate from HG equilibrium values. We note that this cold-QGP alternative has a very comparable statistical significance as the hot-QGP. Given the low temperature and high m_\perp inverse slopes we must have considerable transverse flow. The computed flow velocity at freeze-out is $v_f = 0.51$. This is just below the relativistic sound velocity $v_s = 1/\sqrt{3} = 0.58$, which we have assumed. In

Fig.5 the cross to the left shows the result of the fit we just described; allowing for potentially smaller expansion velocity and all the above discussed uncertainties in the computation, this result must also be seen as a very good agreement between the result of data fit and the theoretical calculation. This also means that we cannot distinguish in the present data between early formation of strange antibaryons and an expansion model followed by direct global hadronization.

Since the fitted values of γ_s and R_C^s allow the HG equilibrium, we attempt such a fit in line 4, where the particle yields are fitted constrained for HG equilibrium, and we use strangeness conservation to evaluate the strangeness fugacity λ_s . We show the result of the fit in the last line of table 4 and in particular we note:

$$\begin{aligned}
T_f &= 155 \pm 7 \text{ MeV}, & \rightarrow v_{\perp} \simeq 0.5 \simeq v_s; \\
\lambda_q &= 1.56 \pm 0.09, & \rightarrow \lambda_s = 1.14; \\
\chi^2/9 &= 0.84, & \rightarrow \text{C.L.} > 60\%.
\end{aligned}
\tag{53}$$

We recall that the baryo-chemical potential is given in terms of T and λ_q , specifically $\mu_b = 3T \ln \lambda_q$, and we find $\mu_b = 204 \pm 10$ MeV in this hadronic gas condition. We note that while the quality of the fit has degraded, it still has considerable statistical significance. It would appear to be a ‘good’ fit to the naked, an unequipped eye.

Unlike S-induced reactions, the hypothesis of an equilibrated HG in the final state cannot be easily discarded in Pb–Pb collisions since the thermochemical parameters are extraordinarily consistent with this hypothesis and the principle of strangeness conservation, as we illustrate in Fig.6. Here, the cross corresponds to the fitted properties of the particle source, while the lines correspond to the constraint of the HG gas source to yield $\langle s - \bar{s} \rangle = 0$ at finite baryon density represented by the value of λ_q . Thus the strange quark fugacity is in general not zero and the cross falls just on freeze-out at $T = 160$ MeV when the meson-baryon abundance is equilibrated. The slight difference in freeze-out value to results shown in last line of table 4 is result of using the WA97 $\bar{\Lambda}/\Lambda$ value Eq.(27) rather than the averred value Eq.(30).

If HG is indeed present in the final state, the proper interpretation of these data, and the likely reaction scenario, compatible with our earlier work on S induced reactions ⁵¹ is as follows; the relatively large fireball of dense and deconfined matter disintegrates and produces dense, confined hadronic gas in which strange particles have time to re-scatter and to establish relative chemical equilibrium. A possible test of this hypothesis would be to see variation of the chemical parameters as the size of the fireball changes with impact parameter (centrality of collision) since re-equilibration should diminish for small

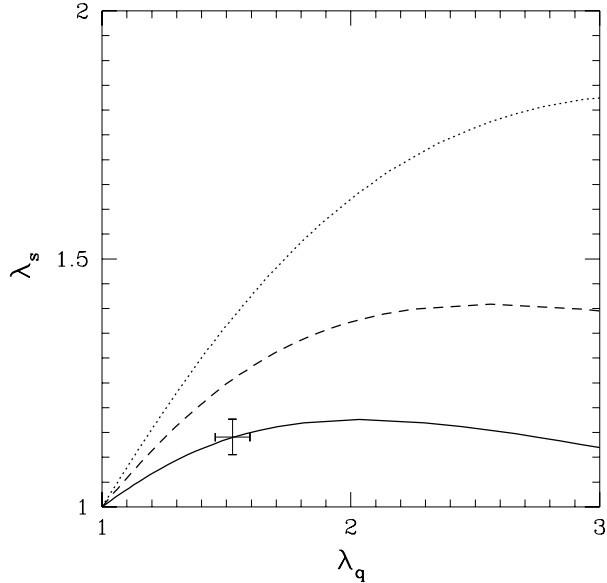


Figure 6: Strangeness conservation constraint in HG as function of freeze-out λ_q : the lines correspond to different freeze-out temperatures T_f (solid 160 MeV, dashed 140 MeV and dotted 120 MeV). The cross corresponds to the chemical freeze-out we determined above.

reaction volume. However, such data are presently not available, and there is no indication that indeed a change of the strange (anti)baryon yields occurs as the centrality of the interaction is reduced. On the other hand, the specific entropy and strangeness should comprise a signal of some new physics should formation and expansion of QGP phase, followed by re-equilibration into HG phase, and freeze-out have occurred. We will now consider the magnitude of these effects:

Strangeness re-equilibration

When HG emerges from initial dense QGP phase, the number of strange quark pairs does not change, but the phase space density of strangeness changes, since the phases are different. Because the HG phase has generally a smaller phase space density of strangeness than QGP, to conserve strangeness, there will be a jump in the phase space occupancy γ_s during the transformation of QGP into HG, as there is a jump in the strange quark fugacity. The important point is that this could lead to significantly overpopulated HG phase ($\gamma_s > 1$). This

phenomenon can be easily quantified as follows: the observed value of γ_s^{HG} is related to the pre-phase change value γ_s^{QGP} by introducing the enhancement factor we wish to determine:

$$\gamma_s^{\text{HG}} \equiv F_\gamma \gamma_s^{\text{QGP}} \quad (54)$$

A simple way to compute the value of the saturation enhancement factor F_γ is to study the abundance of strangeness per baryon number before and after phase transition.

$$F_\gamma = \frac{s/b|_{\text{QGP}}}{s/b|_{\text{HG}}} = \frac{\gamma_s^{\text{QGP}}}{\gamma_s^{\text{HG}}} f(T_f, \lambda_q, \gamma_s^{\text{HG}}). \quad (55)$$

The last expression arises as follows: on the QGP side the abundance of strangeness is to a good approximation proportional to γ_s^{QGP} and is the integral of the strange quark phase space, we evaluate it assuming that $m_s/T_{\text{QGP}} \simeq 1$. There is no dependence on chemical properties of the plasma. On HG side, at freeze-out we have to evaluate the strangeness abundance from the strange particle partition function given in Eq. (16) of ⁵², supplemented by the now relevant term comprising $s\bar{s}$ - η , η' , ϕ states and their resonances. The sum includes a terms proportional to $(\gamma_s^{\text{HG}})^n$, with $n=1, 2, 3$, indicating strangeness content of hadrons. The leading kaon and hyperon term is proportional to γ_s^{HG} and hence we have above result, Eq. (55). We thus obtain, combining Eqs. (54) and Eq. (55),

$$F_\gamma^2 = F_\gamma \frac{\gamma_s^{\text{HG}}}{\gamma_s^{\text{QGP}}} = \frac{s}{\gamma_s b} \Big|_{\text{QGP}} \cdot \frac{\gamma_s b}{s} \Big|_{\text{HG}}, \quad (56)$$

where the right hand side now compares the properties of the two phases at the boundary between them and we can evaluate it using the theoretical equations of state. In analyzes of an experiment we would take the freeze-out parameters determined by the fit to data.

We show, in Fig. 7, the strangeness enhancement factor as function of λ_q for several freeze-out temperatures $T_f = 160, 140, 120$ MeV, with λ_s fixed by strangeness conservation constraint. We see that F_γ varies typically between 1.5 and 2, and is specifically 1.6 for the parameter range of Pb–Pb collisions here discussed. This means that observing the value $\gamma_s \simeq 1$ really means an underlying value $\gamma_s^{\text{QGP}} \simeq 0.6$. Conversely, should we be able to create a longer lived or hotter QGP state we could expect to observe in the HG phase γ_s^{HG} as large as 1.5–2. Such over-saturation of the phase space would be a rather strong smoking gun pointing to the formation of the QGP phase.

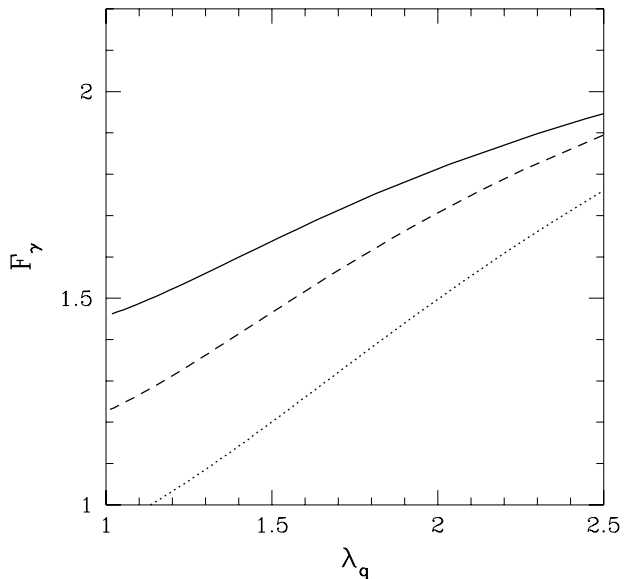


Figure 7: Strangeness phase space enhancement factor as function of HG freeze out λ_q for $T_f = 160$ (solid line), $T_f = 140$ (dashed line), $T_f = 120$ (dotted line). Computed for $\gamma_s^{\text{HG}} = 1$, $m_s/T_{\text{QGP}} = 1$, including in HG phase kaons, hyperons, cascades, η , ϕ , Ω , and imposing strangeness conservation constraint to determine λ_s .

Entropy and particle excess

Another way to argue for the formation of QGP in early stages of an expansion scenario of the fireball is to measure the specific entropy experimentally, for example by measuring the quantity

$$D_Q \equiv \left(\frac{dN^+}{dy} - \frac{dN^-}{dy} \right) / \left(\frac{dN^+}{dy} + \frac{dN^-}{dy} \right), \quad (57)$$

which we have shown to be a good measure of the entropy content⁵⁷. We note that in the numerator of D_Q the charge of particle pairs produced cancels and hence this value is effectively a measure of the baryon number, but there is a significant correction arising from the presence of strange particles. The denominator is a measure of the total multiplicity — its value is different before or after disintegration of the produced unstable hadronic resonances. Using as input the distribution of final state particles as generated within the hadron gas final state it is found³⁸ that $D_Q \cdot S/B$ is nearly independent of the thermal

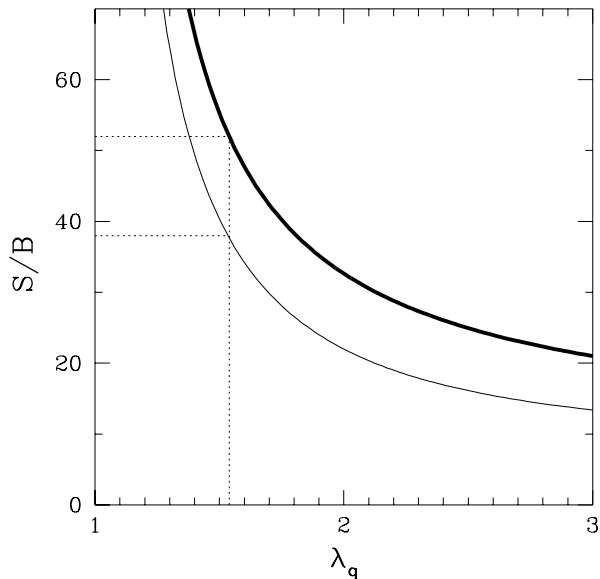


Figure 8: QGP (thick line) and HG (thin line, $T = 155$ MeV) entropy per baryon S/B as function of light quark fugacity λ_q . Dotted lines guide the eye for the here interesting values.

parameters and varies between 4.8, before disintegration of the resonances, to 3 after disintegration.

To obtain a measure of the particle excess, we show in Fig. 8 the specific entropy per baryon S/B content in dense hadronic matter as a function of light quark fugacity λ_q . The thick line addresses the deconfined QGP phase, the thin line the confined HG phase at $T = 155$ MeV, with the strange quark fugacity λ_s being determined from the strangeness conservation condition. While the QGP result is largely independent of temperature (only other, aside of T dimensioned quantity, is m_s), the HG result involves the values of all hadron masses and hence is dependent on T . The 12 units of entropy difference between the two phases for the here interesting range of fugacity $\lambda_q = 1.5$ – 1.6 implies that we should expect an excess of about 3 mesons per baryon if the deconfined phase is formed. We compare with a HG at $T = 155$ MeV; should the HG phase of interest be hotter, this difference between QGP and HG grows, since the baryon density in HG grows much faster than entropy for the baryon mass is well below the temperature range and thus a change in the factor m_N/T

matters, while the change in m_π/T is immaterial. In other work HG phase at 190 MeV is often considered, and there the difference between QGP and HG properties turns out to be as large as factor two³⁸.

6 Discussion and Outlook: QGP

Vacuum and the QCD energy scale

We have relegated to the vacuum properties all scales related to hadronic structure. But where-from are these scales derived? It seems that at present there is indeed no ‘low energy’ practical understanding of the hadronic scale. While ordinary QED matter scale is governed by the atomic Bohr radius $a_0 = \alpha_e^{-1}/m_e$, there is in QCD no obvious relation between quark masses and hadronic spectra and sizes. The scale of the vacuum condensates (see Section 2), and thus of the vacuum condensation energy which results e.g. from the Lattice-QCD approach^{5,17} is a measured property of the physical ground state, and does not relate directly to any fundamental property of the QCD action alone; the Λ_0 -parameter of the strong interaction coupling constant α_s (see Eq. (36) and the middle-section of Fig. 2) has no further meaning, since in fact the strength of this coupling at our energy scale derives from an initial value problem: for a given measured value of α_s at some energy scale, we integrate the renormalization group equations towards the low energy domain (see Section 4) to obtain the needed interaction strength, and the definition of Λ_0 -parameter than arises in terms of the initial values.

It is not the Λ_0 -parameter in the strong coupling constant α_s but the initial point, thus e.g. the grand unification scale, which is defining for us the hadronic energy scale. It is quite possible, though not obvious at all, that Λ_0 establishes the strength of vacuum fluctuations, and thus one would be tempted to conclude that hadronic mass scales are the result of a ‘dimensional transmutation’ mechanism which transports and reduces the grand unification scale to our physical domain. This conclusion is not dependent on the scheme of the unification model employed, so the reader who is not happy with initial value $\alpha_s = \alpha_e$ and the associated huge scales 10^{16} – 10^{18} GeV can equally well use as the input-scale to strong interactions any other initial point, as long as the result yields the now well established experimental value⁴⁵ $\alpha_s(M_Z) \simeq 0.118 \pm 0.03$. It is important here to stress that there is no scenario that would yield the light quark mass as a significant scale, since the scale properties of the physical vacuum always dominate. There is moreover no obvious means to use the masses m_s, m_c which would be easy to associate with QCD condensate scales, since in such an approach there would be no understanding why just two ‘medium’ and not the other quarks determine the scales, nor is there a

noticeable regularity among the mass parameters of matter (quarks, leptons) at any scale²¹.

Nuclear relativistic collisions and strangeness

Considering these strong and unexpected conclusions about the fundamental nature of strong (nuclear) interactions and its far reaching implications, we must assure that the foundations on which these arguments are build are exceptionally solid. The unique tool to study the QCD vacuum is generally accepted to be the process of its change, the ‘micro’ bang in the laboratory. In the relativistic heavy ion collision experiments we seek to prove by finding a way of freeing the color charge of quarks that the effect of confinement arises from quantum fluctuations in the QCD vacuum structure. We hope and expect to produce in these collisions regions of space filled with mobile color charges of quarks and gluons, forming ‘QGP’, the 5th phase of matter comprising a Quark-Gluon (color charge deconfined) Plasma.

Strange particle production is today appreciated as one of the most interesting hadronic observables of dense, strongly interacting matter and much of the current theoretical and experimental effort in study of relativistic nuclear collisions is devoted to this topic. Our work concentrates on the exploration of the pattern of production and evolution of hadronic particles carrying strangeness flavor. Our continued interest in the subject arises from the realization that the experimentally observed anomalous production of (strange) antibaryons cannot be interpreted without introduction of some new physical phenomena, and the hope and expectation is that when more systematic experimental data is available, we will be able to make the argument for deconfinement which will be generally accepted.

In our work we assume that thermal quark-gluon degrees of freedom are at the basis of many of the hadronic particle production phenomena in relativistic hadron reactions. Many simple, but subtle experimental observations point in this natural direction. For example, many of the measured m_{\perp} spectra in S- and Pb-induced reactions have the same shape for strange baryons and antibaryons of the same kind, and even different kinds of particles when considered in same range of m_{\perp} show the same inverse transverse slope (=spectral temperature).

In passing we note that there has been much discussion of the fact that depending on particle mass, the slopes of the particle spectra show different temperatures. This behavior is possibly arising from the fact that for different particles different ranges of m_{\perp} were considered. This is thus evidence for significant expansion flow phenomena governing final stages of QGP disinte-

gration and in no way does this behavior of the spectra contradict the picture of local thermal equilibrium.

We have recently improved the two particle collision cross sections leading to strangeness and charm production. This was done using the recent advances in measurement of the strong coupling constant α_s at the scale of M_Z , a result which eliminated the need for the introduction of an arbitrary coupling constant in flavor production calculations. Using simple dynamical models of dense matter evolution we are able to obtain the final state abundance and phase space occupancy of strangeness originating in the deconfined phase. From this condition at the point that deconfined phase ceases to exist and hadronizes, we develop using conservation laws, constraints on the hadronic particle abundances.

Relative abundances of strange hadrons allowed us to investigate the chemical equilibrium. We find that there is enough time in the collision which passes through the deconfinement phase to establish near-chemical equilibrium conditions locally. The near chemical equilibrium leads to abundance anomalies such as the predicted³⁷ $\bar{\Lambda}/\bar{p} > 1$, found in all A–A collisions⁴⁰. There is a priori no opportunity in terms of reaction mechanisms and time constants for a confined HG state to reach conditions consistent with this result. This result is generally viewed to be a signature for the primordial QGP phase, as such abundances are expected^{37,39} if the HG state of matter has as source the deconfined soup of quarks and gluons.

We did not discuss in depth the entropy excess (see, however, our earlier report⁶), which also are inconsistent with pure HG state, but are well understood in terms of deconfinement.

Our view is that the observed hadronic particle effects, and specifically strangeness, provide a simple, consistent interpretation of the heavy ion collision data within the hypothesis that a novel type of deconfined hadronic matter is formed in both S- and Pb-induced reactions on heavy nuclei, but that quite different initial conditions are reached in these two cases. Moreover, the longitudinal flow, clearly visible in the S–S 200A GeV, in *e.g.*, Λ -rapidity spectra, is not as pronounced in Pb–Pb reactions, but there seems to be relatively strong transverse/radial flow driven by the high internal pressure which has been reached in the initially highly compressed fireball matter. We also expect that the much greater volume of the fireball formed in Pb–Pb reactions, as compared to S–Pb leads to a greater volume of deconfined initial phase, which in turn in the hadronization process should enhance the re-equilibration of final state hadrons after freeze-out. Thus the Pb–Pb collisions should more approach the HG type chemical equilibrium of particle yields than S–W/Pb or S–S reactions.

The only potentially contradiction to this unified view of the 160–200 GeV heavy ion reactions may be the systematics of charmonium production which suggest a difference in the absorption rate of $c\bar{c}$ in central dense matter formed in Pb–Pb interactions as compared to the earlier studies of pA and SA collisions. There is no full and consistent theoretical understanding of all experimental details which may yet turn out to confirm our views about the presence of deconfinement in all these conditions.

Immediate future

Underlying the strange particle signatures of deconfinement is the rather rapid chemical equilibration of quark flavor, originating in gluon fusion reactions. Gluons themselves are the QGP fraction which is generally believed to most rapidly approach chemical equilibrium in the deconfined phase. We presumed in our studies that at SPS energies that gluon chemical equilibrium has been reached, considering the lifespan of the reaction. Such an assumption is less compelling at RHIC energies, indeed some model calculations exist arguing that even gluons could not reach full equilibrium. These conclusions are reached assuming a fixed and small QCD interaction strength α_s . Since there is no threshold to production of gluons, and Bose effects enhance in dense matter gluon formation, our study of the strong scale dependence of α_s suggest that one has to review the gluon chemical equilibration in the near future. In anticipation of this, we recommend use of glue chemical equilibrium for RHIC energy scale collisions as well.

The dynamics of evolving and exploding QGP phase impacts significantly the resulting entropy distribution in rapidity and strange particle abundances. At present we have also engaged in several approaches to the explosive flow problem: we study 3-d hydrodynamic solutions, develop semi-analytically soluble homologous hydrodynamic evolution/flow models of QGP and study the entropy sources during the flow phase. Our schematic approach⁴⁹ will permit by its simplicity a systematic investigation of the complex dynamics of strongly interacting hadronic matter evolution comprises several interwoven challenges:

- a) the determination of initial flow conditions;
- b) description of explosive flow of dense matter and the radiation reaction;
- c) influence on matter flow by the equations of state
- d) constrains on the final state conserved quantities (baryon number, entropy, and strangeness).

While hydrodynamical flow of thermally equilibrated matter is not entropy producing, other dynamical processes occur during the evolution of dense matter that can produce entropy, for example chemical equilibration, i.e. approach

of particle abundances to their equilibrium number is entropy producing. We consider of considerable importance that relativistic hydrodynamical dynamical flow equations are improved to allow for entropy production by approach to phase space saturation by gluons and quarks.

The key problem we need to resolve is how to establish that we have indeed seen the thermal, deconfined phase, where the degrees of freedom are those of nearly massless quarks and gluons? Other forms and phases of hadronic matter can perhaps yet be invented that could produce similar observational effects. We need to devise experimental approaches that would allow us to understand the rich deconfinement properties of dense relativistic nuclear/quark matter. In immediate future we have to explore the collision energy dependence and see how the key properties change between the low AGS energies, the intermediate SPS energies towards the immediate future of RHIC.

Acknowledgments

I would like to take this opportunity to thank my Brazilian colleagues:

Prof. Carlos E. Aguiar of UFRJ;
Dr. Sergio B. Duarte of CBPF;
Prof. Chung K. Cheong of UERJ/CBPF;
Prof. Yojiro Hama of IF-USP; and the chairman,
Prof. Takeshi Kodama of UFRJ

for putting together this most stimulating and exciting week in Rio. I am sure that not just me, but we all, have immensely enjoyed a rare combination of the warm carioca spirit at the foot of the Pão de Açúcar, with an intense, cutting edge, meeting program which brought us from far away together, kept us on the tip-toes all day and left us no time to breath.

This report is dedicated to the many young participants at the workshop. Their enthusiasm was exemplary, and their interest and commitment strengthened my resolve to compose a comprehensive write-up of my lecture. In doing so I have drawn on some material⁴⁷ developed originally together with my long-time collaborators, and I would like to thank in particular J. Letessier and A. Tounsi from LPTHE-University Paris 7 for their kind support in our quest for strange particle signatures of QGP.

In the course of preparation of these notes I greatly benefited from interactions and comments made by Takeshi Kodama. I would like to thank him warmly for many valuable suggestions, and a careful reading of the manuscript draft.

This research program is supported by US-Department of Energy under grant DE-FG03-95ER40937.

1. C. Lattes, G. Occhialini and C. Powell, *Nature* **159**, 93, 186, 694 (1947); **159** 453, 486 (1947);
E. Gardner and C.M. G. Lattes, *Science* **107**, 271 (1948).
2. H. Fritzsche, M. Gell-Mann and H. Leutwyler, *Phys. Lett.* **47 B**, 365 (1973);
H.D. Politzer, *Phys. Rep.* **14**, 129-180 (1974) (see p.154 and Refs. 34-41).
3. S. Weinberg, *The Quantum Theory of Fields I + II* Cambridge, University Press, 1995/96.
4. T.D. Lee, *Particle Physics and Introduction to Field Theory*, Harwood, New York 1982.
5. C. DeTar, *Quark Gluon Plasma in Numerical Simulations of Lattice QCD*, in *Quark Gluon Plasma 2*, p.1, R.C. Hwa (Eds.), World Sci., (Singapore 1995).
T. Blum, L. Kärkkäinen, D. Toussaint, S. Gottlieb, *Phys. Rev.* **D51**, 5153 (1995).
6. J. Rafelski, J. Letessier, and A. Tounsi, “Flavor Flow Signatures of Quark-Gluon Plasma”, in *Relativistic Aspects of Nuclear Physics*, Eds. T. Kodama et al., p. 211, World Scientific, (Singapore 1996).
7. G. Soff, B. Müller, J. Rafelski and W. Greiner, *Z. Naturf.* **28a**, 1389 (1973).
8. E. Fermi, *Prog. Theo. Phys.* **5**, 570 (1950); *Phys. Rev.* **81**, 570 (1951).
9. L.D. Landau, *Izv. Akad. Nauk SSSR, Ser. Fiz.* **17**, 51 (1953);
L.D. Landau and S.Z. Belenkij, *Usp. Phys. Nauk*, **56**, 309 (1956); also *Nuovo Cim. Suppl.* **3**, 15 (1956);
These articles have been reprinted in English translation in *Collected Papers of L.D. Landau*, Gordon and Breach, D. Ter Haar, Ed. (New York, 1965).
10. R. Hagedorn, *Suppl. Nuovo Cimento* **2**, 147 (1965).
R. Hagedorn, *Cargèse lectures in Physics*, Vol. 6, Gordon and Breach (New York 1977) and references therein.
See also many contributions in: J. Letessier, H. Gutbrod and J. Rafelski, *Hot Hadronic Matter*, Plenum Press NATO-ASI series B346 (New York 1995).
11. R. Hagedorn and J. Rafelski, *Phys. Lett.* **97B**, 136 (1980);
R. Hagedorn, I. Montvay and J. Rafelski, *Thermodynamics of Nuclear Matter from the Statistical Bootstrap Model* in: *Hadronic Matter at Extreme Energy Density*, N. Cabibo and L. Sertorio, eds. (Plenum Press, 1980).
12. A. Chodos, R.L. Jaffe, K. Johnson, C.B. Thorn, and V. Weisskopf, *Phys. Rev.* **D9**, 3471 (1974);
A. Chodos, R.L. Jaffe, K. Johnson, and C.B. Thorn, *Phys. Rev.* **D10**, 2599 (1974);
K. Johnson, *Acta Phys. Pol.* **B6**, 865 (1975).
13. P. Carruthers, *Collective Phenomena*, **1**, 147 (1973).
14. R. Hagedorn and J. Rafelski in: *Statistical Mechanics of Quarks and Hadrons*, H. Satz, ed., North Holland, (Amsterdam 1981) p. 237 and p. 253. J. Rafelski *Phys. Rep.* **88**, 331 (1982).

15. M.A. Shifman, A.I. Vainshtein and V.I. Zakharov, *Nucl. Phys.* **B147** (1979) 385; 448; 519.
16. *Vacuum Structure and QCD Sum Rules*, M. A. Shifman, ed., North Holland, Amsterdam 1992.
17. M. D'Elia, A. Di Giacomo, and E. Meggiolaro, *Phys. Lett.* **B408**, 315 (1997); and in *proc. of "XVth International Symposium on Lattice Field Theory", Edinburgh (UK), July 22-26, 1997 (LATTICE 97) Nucl. Phys. Proc. Suppl.* **63** 465 (1998) [hep-lat/9709031].
18. S. Narison *Phys. Lett.* **B387**, 162 (1996); **B358**, 113 (1995).
19. S. Klevansky, *Rev. Mod. Phys.* **64**, 649 (1992).
20. H.G. Dosch and S. Narison *Phys. Lett.* **B417**, 173 (1998); [hep-ph/9709215].
21. H. Fusaoka and Y. Koide, *Phys. Rev.* **D57**, 3986 (1998); [hep-ph/9712201].
22. M.S. Dubovikov and A.V. Smilga, *Nucl. Phys.* **B185** 109 (1981).
23. J. Soto *Phys. Lett.* **B165**, 389 (1985).
24. G.V. Efimov, S.N. Nedelko *Eur.Phys.J.* **C1**, 343 (1998); [hep-ph/9607424]
25. E. Elizalde and J. Soto, *Z. Phys.* **C31**, 237 (1986).
26. J. Schwinger, *Phys. Rev.* **82**, 664 (1951).
27. H. Euler and B. Kockel, *Naturwissenschaften.*, **23**, 246 (1935);
W. Heisenberg, *Z. Phys.* **90**, 209 (1935);
W. Heisenberg and H. Euler, *Z. Phys.* **98**, 714 (1936).
28. J. Rafelski, L. Fulcher and A. Klein, *Phys. Rep.* **38**, 227 (1978), and refs therein.
29. H.G. Dosch, *Phys. Lett.* **B190**, 177 (1987).
30. H.G. Dosch, *Prog. Part. Nucl. Phys.* **33** 121 (1994).
31. T. deGrand, R.L. Jaffe, K. Johnson, and J. Kiskis, *Phys. Rev.* **D12**, 2060 (1975).
32. A.T.M. Aerts and J. Rafelski *Phys. Lett.* **148B**, 337 (1984).
33. K. Johnson, *Acta Phys. Pol.* **B6**, 865 (1975).
34. F. Buccella, G.F. Farrar, and A. Pugliese, *Phys. Lett.* **B153**, 311 (1985).
35. R.L. Jaffe *Phys. Rev.* **D15**, 281 (1977).
36. G. Baym, lecture at this meeting;
U. Heinz, lecture at this meeting.
37. J. Rafelski, *Phys. Rep.* **88**, 331 (1982).
38. J. Rafelski, J. Letessier and A. Tounsi, *XXVI International Conference on High Energy Physics*, Dallas, (1992) AIP-Conference Proceedings No 272, J.R. Sanford, ed., p. 272;
J. Letessier, A. Tounsi, U. Heinz, J. Sollfrank and J. Rafelski, *Phys. Rev. Lett.* **70**, 3530 (1993).
39. P. Koch, B. Müller, and J. Rafelski, *Phys. Rep.* **142**, 167 (1986); *Z. Phys.* **A324**, 453 (1986).
40. T. Alber *et al.*, NA35 collaboration, *Phys. Lett* **B366**, 56 (1996).
41. I. Králik, WA97 Collaboration, CERN presentation May 12/13, 1997, *Hyperon and Anti hyperon Production in Pb-Pb Collisions at 158A GeV/c*, in⁵⁹.
42. Ch. Bormann, NA49 Collaboration, *Kaon, Λ , and $\bar{\Lambda}$ -Production in Pb+Pb*

- Collisions at 158 GeV per Nucleon*, IKF-Frankfurt report, May 1997, in ⁵⁹.
43. I. Hinchliffe, "Quantum Chromodynamics", in: L. Montanet *et al.*, Phys. Rev. **D54** (1996) 1; see also:
T. Muta, *Foundations of Quantum Chromodynamics*, World Scientific (Singapore 1987).
 44. L.R. Surguladze and M.A. Samuel, *Rev. Mod. Phys.* **68**, 259 (1996).
 45. M. Schmelling, *Status of the Strong Coupling Constant*, in proc. of ICHEP 1996, World Scientific, Singapore 1997, Z. Ajduk and A.K. Wróblewski, eds., p. 91;
S. Bethke, *Nucl. Phys. Proc.Suppl.* **64**, 54 (1998) [hep-ex/9710030].
 46. J. Letessier, J. Rafelski, and A. Tounsi, *Phys. Lett.* **B389**, 586 (1996).
 47. J. Letessier, J. Rafelski, and A. Tounsi, *Acta Phys. Pol.* **B28**, 2841 (1997).
 48. P. Elmfors and R. Kobes, Phys. Rev. **D51** (1995) 774.
 49. H.Th. Elze, Y. Hama, T. Kodama, M. Makler and J. Rafelski, *Variational Principle for Relativistic Fluid Dynamics*, in preparation.
 50. J. Letessier, J. Rafelski and A. Tounsi, *Phys. Lett.* **B321**, 394 (1994); **B323**, 393 (1994); **B333**, 484 (1994); **B390**, 363 (1997).
 51. J. Rafelski, J. Letessier and A. Tounsi, *Acta Phys. Pol.* **B27**, 1035 (1996).
 52. J. Letessier, A. Tounsi, U. Heinz, J. Sollfrank and J. Rafelski, *Phys. Rev.* **D51**, 3408 (1995).
 53. G. Odyniec, NA49 Collaboration, $\Xi(\Omega)$ Production in Pb+Pb Collisions at 158 GeV/c, Preprint LBL-40422, June 1997, in ⁵⁹.
 54. I.G. Bearden *et al.*, NA44 Collaboration, *Phys. Lett.* **B388**, 388 (1996). I.G. Bearden *et al.*, NA44 Collaboration, *Phys. Rev. Lett.* **78**, 2080 (1997).
 55. E. Shuryak and V. Thorsson, *Nuc. Phys.* **B536**, 739 (1992).
 56. C. Gong, *J. Phys. G: Nucl. Part. Phys.* **18**, L123 (1992).
 57. J. Sollfrank, M. Gaździcki, U. Heinz and J. Rafelski, *Z. Physik* **C61**, 659 (1994).
 58. S. Abatzis *et al.*, WA85 Collaboration, *Phys. Lett. B* **376**, 251 (1996).
 59. A.D. Panagiotou *et al.*, Proceedings of SQM'97 meeting, Thera, Greece, 1997.